Improving Geologic and Engineering Models of Midcontinent Fracture and Karst-Modified Reservoirs Using New 3-D Seismic Attributes

Type of Report: Semiannual Scientific/Technical

Reporting Period Start Date: October 1, 2006

Reporting Period End Date: March 31, 2007

Principal Authors:

Susan E. Nissen, Consultant, McLouth, Kansas
Saibal Bhattacharya, Kansas Geological Survey, University of Kansas, Lawrence, Kansas
John Doveton, Kansas Geological Survey, University of Kansas, Lawrence, Kansas
W. Lynn Watney, Kansas Geological Survey, University of Kansas, Lawrence, Kansas

Contributors:

Alan P. Byrnes, Kansas Geological Survey, University of Kansas, Lawrence, Kansas
Kurt Marfurt, Allied Geophysical Laboratories, University of Houston, Houston, Texas
E. Charlotte Sullivan, Pacific Northwest National Labs, Richland, Washington

Date Report was Issued: June 2007

DOE Award Number: DE-FC26-04NT15504

Submitting Organizations:

The University of Kansas Center for Research, Inc
2385 Irving Hill Road
Lawrence, Kansas 66045-7563

Allied Geophysical Laboratories
Department of Geosciences
University of Houston
Houston, Texas 77204-5505

DISCLAIMER

ABSTRACT

The goal of our project is to develop innovative seismic-based workflows for the incremental recovery of oil from karst-modified reservoirs within the onshore continental United States. Specific project objectives are: (1) to calibrate new multi-trace seismic attributes for improved imaging of karst-modified reservoirs, (2) to develop attribute-based, cost-effective workflows to better characterize karst-modified carbonate reservoirs and fracture systems, and (3) to improve accuracy and predictiveness of resulting geomodels and reservoir simulations. In order to develop our workflows and validate our techniques, we are conducting integrated studies, including reservoir characterization, geomodel building, and reservoir simulation, of three karst-modified reservoirs: the Permian San Andres in west Texas, the Mississippian Spergen in Colorado, and the Ordovician Arbuckle in Kansas.

During this fifth reporting period, from October1, 2006, through March 31, 2007, new interpretations have enhanced the reservoir characterizations for all three study areas. We have generated a geomodel for the Spergen reservoir in the northern portion of the Mississippian study area, incorporating compartment boundaries defined using volumetric curvature attributes, and reservoir simulation of one of these compartments suggests that the curvature-defined reservoir compartments are reasonable. Based primarily on our work in the three study areas, we have developed a best practices workflow for using geometric seismic attributes such as volumetric curvature to characterize reservoirs modified by karst.

Technology transfer of our project work to date has been accomplished through presentations at professional society meetings and associated publications, Kansas Geological Survey Open-file reports, Master's theses, and postings on the project website: http://www.kgs.ku.edu/SEISKARST.

TABLE OF CONTENTS

EXECUTIVE SUMMARY

We are conducting integrated studies of three karst-modified reservoirs: the Permian San Andres in west Texas, the Mississippian Spergen in Colorado, and the Ordovician Arbuckle in Kansas in order to develop innovative seismic-based workflows for the incremental recovery of oil from karst-modified reservoirs within the onshore continental United States. During this fifth reporting period, from October 1, 2006, through March 31, 2007, our project was focused on the following tasks: (1) integrated reservoir characterization; (2) geomodel construction; (3) reservoir simulation; and (4) synthesis of a best practices workflow for using seismic attributes (primarily geometric attributes) to characterize reservoirs modified by karst. New results are described below:

Permian San Andres Study Area. The focus of this phase of the reservoir analysis of the "high volume area" at Waddell Field has been to 1) identify and characterize the karst distribution of the San Andres Formation in the "high volume area" and 2) provide a first approximation of the porous San Andres beneath the upper karst interval using log, core, and seismic data. Core data indicate that the "high volume area" consists of 1) non porous "macro" karst, characterized by intense chaotic brecciation and anhydrite replacement, and 2) bedded gypsiferous oolitic, fusulinid, and skeletal packstone and grainstone reservoir rock. The non porous and anhydritic karst were quantitatively discriminated from the lower packstone-grainstone strata in wells using wireline log petrophysical solutions. Two log variables were used independently to estimate the base of the anhydrite zone: porosity obtained from the sonic log and the anhydrite content estimated from the density, neutron porosity, and photoelectric factor curves. A zonation program was used to locate stratal boundaries where variability is maximized between the zones. Results of the petrophysical analysis of the karst were depicted in maps, which were compared to the structure on top of the San Andres and its 4^{th}-order trend residual. The tight and anhydritic zones exhibit high variability in thickness; however both generally thicken on the higher portions of the SE-trending anticline that runs through the "high volume area". A preliminary examination of the general porosity development within the underlying grainstone-packstone reservoir-bearing interval showed that thicker porous carbonate development is focused on the saddle area of the SE-trending anticline. Also, depth to the base of porous carbonate is greater along this saddle area of the structure, suggesting a structural influence. A model-based impedance inversion of the seismic amplitude volume in the "high volume area" was generated in order to improve seismic interpretations. Using this impedance volume, a horizon that approximates the top of the San Andres Formation can be interpreted across the "high volume area". Detailed comparison to well tops indicates that this horizon actually corresponds to the base of the anhydritic karst interval. An underlying seismic horizon, apparently corresponding to the base of the porous reservoir, is truncated by the base of karst in some areas. During the next reporting period, we will attempt to identify if there is a difference in reservoir type/quality in areas where this horizon is absent.

Mississippian Spergen Study Area. Our primary focus during this reporting period has been detailed reservoir modeling for the southern portion of Smoky Creek field. There is

significant variation in well productivity in this field, where most wells are drilled on 40-acre (16-hectare) spacing. Based on standard log analysis and 40-acre (16 hectare) drainage, some of the wells show more than 100 percent recovery. Volumetric curvature analyses of 3-D seismic data reveal the presence of possible compartments of various sizes in the reservoir. The compartments are defined using a most positive curvature extraction. One of the larger compartments, containing two productive wells, was characterized and simulated to validate if such a drainage volume could support the historic production and pressure performance of the constituent wells. Initial results show reasonable history matches of both production and pressure for these two wells. Lacking core data from Smoky Creek, permeability was estimated by reconciling log-derived water saturation and generalized capillary pressure formulation for Mississippian rocks. A permeability multiplier of 3 was required to obtain the history matches at the modeled wells. However, a 2 porosity unit increase in formation porosity (within the observed error in log to core porosity comparisons from nearby Cheyenne Wells field) would also raise the estimated permeability into the range required to obtain performance history matches. Future work includes simulation of all the compartments containing wells to show if the remaining compartments delineated from volumetric curvature analyses are realistic. If simulation of these compartments is successful, we will also model the potential for additional resources in untapped compartments.

Arbuckle Study Area. The goal of our work during the present reporting period has been to begin detailed reservoir characterization of the Arbuckle within the seismic survey area. Wireline log data have been used to estimate the oil/water contact and the porosity distribution of the uppermost Arbuckle within this area. The log-defined oil-water contact varies across the seismic survey area by up to 25 ft (8 m), suggesting variation in the petrophysical properties of the uppermost Arbuckle across the study area. Pickett plots of three wells in two structurally defined compartments confirm lateral variation in the Arbuckle reservoir properties. Wells in one compartment show a coarsening upward trend, high water saturations (>60%), and irreducible BVW of approximately 0.068, while the well in the other compartment shows a tight interval with small pore size at the top of the Arbuckle underlain by a relatively uniform layer with water saturation as low as 45%, and an irreducible BVW of approximately 0.055. In addition to these observed changes in reservoir properties between compartments, the data show variations in reservoir quality within a single compartment.

Based primarily on our work in the three study areas, we have developed a best practices workflow for using seismic attributes to characterize karst-modified reservoirs. Our best practices workflow suggests that integrating geologic data with information from seismic horizon structure and volumetric attributes allows us to classify the type of karst overprint and to distinguish tectonic features from karst features. This methodology can provide insight on origin of observed features and may help identify uncertainties in reservoir quality, compartmentalization, and seal integrity.

Technology transfer of our project work to date has been accomplished through presentations at professional society meetings and associated publications, Kansas Geological Survey Open-file reports, Master's theses, and postings on the project website: http://www.kgs.ku.edu/SEISKARST.

1.0 INTRODUCTION

The overall goal of our project is to develop innovative seismic-based workflows for the incremental recovery of oil from karst-modified reservoirs within the onshore continental United States. Specific project objectives are: (1) to calibrate new multi-trace seismic attributes for improved imaging of karst-modified reservoirs, (2) to develop attribute-based, cost-effective workflows to better characterize karst-modified carbonate reservoirs and fracture systems, and (3) to improve accuracy and predictiveness of resulting geomodels and reservoir simulations. In order to develop our workflows and validate our techniques, we are conducting integrated studies of three karst-modified reservoirs: the Permian San Andres in west Texas, the Mississippian Spergen in Colorado, and the Ordovician Arbuckle in Kansas (Figure 1.1).

In the first four reporting periods, from October 1, 2004, through September 30, 2006, we (1) gathered 3-D seismic, petrophysical, and engineering data; (2) generated multi-trace seismic attribute volumes (including coherence and volumetric curvature attributes) for the 3-D seismic surveys; (3) generated a preliminary seismic attribute catalog of karst features (available online at http://www.kgs.ku.edu/SEISKARST/catalog.html); (4) conducted reservoir characterization studies (seismic, geological, petrophysical, and engineering); (5) developed and implemented a workflow for geomodel building; and (6) provided technology transfer through presentations at professional society meetings and associated publications, in Kansas Geological Survey Open-file reports, and via postings to our project website (http://www.kgs.ku.edu/SEISKARST).

During this fifth reporting period, from October 1, 2006, through March 31, 2007, we focused on the following tasks: (1) integrated reservoir characterization; (2) geomodel construction; (3) reservoir simulation; and (4) synthesis of a best practices workflow for using seismic attributes (primarily geometric attributes) to characterize reservoirs modified by karst (Figure 1.2). Details of the accomplishments for the October 1, 2006, to March 31, 2007 reporting period are documented below.

2.0 PERMIAN SAN ANDRES STUDY AREA

The Permian San Andres study area is approximately 5 square miles (13 square kilometers) in size and covers the "high volume area" of Waddell Field, Crane County, Texas, located on the east central flank of the Central Basin Platform of the Permian Basin. This "high volume area" is characterized by variable fluid production, but overall fluid production is an order of magnitude greater than in surrounding areas of the field. Operator-interpreted tracer and pressure data indicate a highly compartmentalized reservoir with an active water drive. Reservoir heterogeneity appears to be related to stratigraphy and diagenesis, as well as anhydrite-cemented karst features associated with the subaerial exposure surface developed on the top of San Andres Formation.

The focus of this phase of the reservoir analysis of the "high volume area" at Waddell Field is to 1) identify and characterize the karst distribution of the San Andres Formation in the "high volume area" and 2) provide a first approximation of the porous San Andres

Formation beneath the upper karst interval using log, core, and seismic data. In addition, the general distribution of the porous interval is compared to karst development to determine interrelationships that may be important for assessing the impact of karst development on the nature of flow barriers and pathways. Maps and cross sections of well data are compared with seismic data in an attempt to define interwell distribution of karst and the configuration of the underlying San Andres formation. Quantitative analysis of effective porosity and fluid saturations will be analyzed during the next reporting period.

2.1 Geological Characterization

The configuration of the top of the San Andres Formation serves as a base map for the "high volume area" in Waddell Field (Figure 2.1). This map has been updated from that shown in the November 2006 Semiannual Scientific/Technical Report, based on revised picks of the top of San Andres Formation using well logs. A southeast-trending plunging anticline approximately two miles long crosscuts the mapped area, showing a relief of approximately 75 ft (23 m) and a width of approximately one mile (1.6 km). The northwest portion of the mapped area is structurally higher, with a shallow saddle in the central mapped area. The correlation of the top is generally straightforward due to the usual presence of a thin, but distinctive, shaly interval developed at the base of the overlying Grayburg Formation (Figure 2.2). However, local areas are missing this shale and increase the difficulty in distinguishing the top of the San Andres Formation on logs.

Cross section A-A' in Figure 2.2 illustrates correlations between two cored wells, Waddell #1261 and #1204, within 1 mile (1.6 km) of each other. Correlations suggested by the operating company illustrate complex relationships of the perforated intervals involving karst at the top of the San Andres Formation and the porous oolitic shoal lithofacies immediately beneath the karst. Core descriptions indicate that the upper karst interval in these wells (purple highlight) involves macroscopic collapse and chaotic brecciation and extensive anhydrite replacement of gypsum in the upper San Andres Formation. In contrast, what is identified as porous karst and karsted shoal below the main karst zone in Waddell #1204 is less intensely karsted, without macro-scale chaotic brecciation and anhydrite replacement. This cm-scale dissolution and brecciation is recognized here as "micro" karst where the matrix (fusulinids-ooid-skeletal packstone in well #1204) is essentially intact. The matrix properties in the microkarsted intervals are also probably dominant in terms of fluid flow. Thus, these lower zones, the "porous karst zone" and the "karsted and bioturbated fusulinid shoal" in well #1204, are placed in the *in situ* bedded carbonate reservoir of the San Andres Formation. The higher porosity in these lower zones is also more consistent with the "matrix" reservoir of the porous San Andres Formation lying beneath the karst. Using this two-tier karst classification based on intensity and scale results in a better correlation between both the upper intensely macrokarst and less porous intervals and the higher porosity zones of grainstone and packstone below the major karst interval. Distinguishing the intensity and scale of the karst, e.g., via petrophysical estimates of anhydrite distribution, may help understand the origin of this karst.

Cross section A-A' is modified to include two informal stratigraphic markers. The yellow dashed line delineates the top of a tighter zone beneath the first higher porosity zone, and the "x" marker, shown as a blue dashed line, is identified at the base of the main porosity interval that contains a majority of the production perforations. The "x" marker lies consistently approximately 150 feet (46 m) below the top of San Andres Formation. Additional discussion of the stratigraphy of the San Andres is provided below.

2.1.1 Stratigraphy and Lithofacies Succession

The gross producing interval in the Waddell Field "high volume area" falls within the uppermost 150 feet (46 m) of the top of the San Andres Formation, above the "x" marker described above. Prior regional stratigraphic analysis based on surface exposures (~100 mi (160 km) to the west) and seismic data in the vicinity of the field have established a sequence and seismic stratigraphic framework of the San Andres Formation, including recognition of high frequency sequences (HFS) (French and Kerans, 2004). The Waddell Field San Andres reservoir lies within the Guad 8 and overlying Guad 9 sequences. Guad 8 and Guad 9 are examples of HFS and together comprise a sequence set that exhibits retrogradational to aggradational to progradational stratal stacking geometries (French and Kerans, 2004). The sequence set is expressed in the high volume area as a longer-term shallowing upward succession of cyclic bioclastic dolo-wackestones to oolitic (oomoldic) to fusulinid dolo-grainstones and packstones. These strata were deposited along a shallow, eastward sloping ramp of the eastern margin of the Central Basin Platform.

In the high volume area, the regional stratal boundary that separates the underlying Guad 8 from Guad 9 has not been precisely located and tied into the regional framework. However, preliminary log correlations delimit informal stratigraphic markers within the San Andres Formation. While still tentative, in part due to lack of core data for this interval, the "x" marker described above may be equivalent to the boundary between Guad 8 and Guad 9, since the next underlying HFS boundary is between Guad 4 and Guad 8. This "G4" boundary is known to reside below the depths of the "x" marker, based on seismic correlations.

Core descriptions of Waddell #1261 and #1204 indicate that the upper karst interval in these wells (highlighted as purple in Figure 2.2) is a macro karst consisting of large clasts and blocks of strata, blocks much larger than the core diameter. The karst is recognized by 1) extensive macro chaotic brecciation, dissolution, and collapse of the bedded oolitic, fusulinids, skeletal grainstone/packstone succession that typifies the upper San Andres Formation; 2) occlusion of considerable amounts of matrix-based oomoldic, moldic, and vug porosity by varying amounts of anhydrite and gypsum; and 3) extensive replacement of gypsum by anhydrite. This macro karst represents extensive dissolution, large void formation, and stratal disruption that is associated with the uppermost surface of the San Andres Formation.

The shoal-water, oolitic, fusulinid, skeletal grainstones and packstones are characterized by biomoldic and oomoldic porosity with scattered vugs and fractures. The pore space is partly occluded by gypsum, making distinction of true pore space difficult due to the low

bulk density of gypsum and its waters of hydration. The task of discriminating actual pore space was initiated in this reporting period with log compositional analysis, but will be the focus in the next reporting period.

The low porosity anhydritic karst in the upper portion of the San Andres Formation in Waddell Field is irregularly developed beneath (up to 100 ft or 30 m) the top of San Andres Formation and has a lateral distribution that is poorly understood. The nature of this karst surface is an important objective of this project. Porosity in the karst is generally developed in thin (<10 ft or 3 m) intervals, but is irregularly distributed through the karst. For the most part, the karst apparently destroyed most of the earlier matrix porosity, primarily oomoldic, biomoldic, and vuggy porosity and accordingly, the karst serves as a probable vertical barrier to lateral flow.

The karst appears to be closely linked to subaerial exposure in association with the unconformity at the top of the San Andres Formation and the Guad 8-9 composite depositional sequence. However, later hydrothermal processes associated with tectonic fracture systems are believed to have dissolved out anhydrite cement in certain locations. This late-stage overprint leads to additional complexities in the present distribution of the anhydritic karst.

The resulting complex distribution of karst and its general non or marginal reservoir properties significantly affected spatial distribution and continuity of hydrocarbon pay in Waddell Field. Intervals of production perforations and production strategies used to develop Waddell Field are highly variable and have met varying success. Limited tracer surveys indicate considerable directional flow and limited communication, at least over the short periods where tracers are measured.

Petrophysical characterization of the karst was done as a first step to relate and extend karst as it is observed in core to its discrimination on well logs. This work is presented in the next section. Mapping of these results are including in a subsequent section of this report.

2.1.2 Petrophysical discrimination of the low-porosity anhydritic karst zone at the top of the San Andres Formation

The evaluation of the San Andres Formation in the W. N. Waddell #1261 subdivided the cored interval between an upper karst zone in which porosity had been occluded by anhydrite and a lower, porous oolitic shoal lithofacies. As described in the November 2006 Semi-Annual Scientific/Technical Report, a porosity-multimineral transformation of density, neutron porosity, photoelectric factor, and sonic logs showed excellent concordance with core descriptions and porosity measurements in this well. In particular, the high content of anhydrite and low porosity of the karst zone was strongly differentiated from the more porous section below the karst which also appeared to be more gypsiferous. Application of the log mineral transform to other, uncored wells in the field commonly showed a similar motif of a low-porosity anhydritic zone at the top of the San Andres which could be interpreted as karstic, based on core studies from Waddell #1261. The lower boundary of the interpreted karst zone showed high variability, so that

its thickness showed good lateral continuity in some areas, but punctuated by anomalies where either the "karstic" interval was markedly thick or where it was thin or appeared to be absent.

Two log variables were used independently to estimate the base of the anhydrite zone: the sonic log and the anhydrite content estimated from the density, neutron porosity, and photoelectric factor curves. The sonic log was used as a generalized porosity log, both because its response is least affected by mineral changes (Holz et al, 2002) and also because a major subdivision based on this acoustic measurement could be tied more directly to seismic property evaluation. The lower boundary of the karst zone was calculated by a zonation program which locates zone boundaries such that variability is maximized between the zones while minimizing variability within the zones (Bohling et al, 1998). The application of a statistical program provides a consistent boundary location method but it is also based on the aggregate statistics of the section, rather than localized features and so is therefore more likely to be matched with the coarse averaging of seismic properties.

An example of the results of the karstic zone methodology are shown in Figure 2.3 for the cored Waddell #1261 well and two neighboring wells. In Waddell #1261, the core description subdivision of the upper San Andres Formation between the karst zone and porous, oolitic shoal facies is closely matched by the zonation picks based on the sonic and estimated-anhydrite logs. The porosity-anhydrite-gypsum curves in Waddell #1207 show a similar structure to Waddell #1261, but the karstic zone is thinner. However, in Waddell #1228, the interpreted karstic zone appears to have a much thicker development of about 100 feet, based on both the sonic and anhydrite curves. Notice that the zone has a layered structure of alternating low-porosity anhydritic dolomite and gypsiferous dolomite. The greater thickness and layering suggests a more complex genesis in karsting coupled with other processes in the upper San Andres Formation in this well.

Statistical zonation estimates of the depth of the base of the low-porosity zone and anhydrite phase at the top of the San Andres Formation were compiled for all wells with density, neutron, photoelectric factor, and sonic logs. The average anhydrite content of the low-porosity zone was also computed. In some wells, where only a sonic log was available, the estimate was restricted to the base of the low-porosity section. In a few wells, there was no evidence of a low-porosity, anhydritic zone at the top of the San Andres and this was interpreted as an absence of karst development.

2.1.3 Mapping

A revised map of the 4th-order trend surface residual for the top of the San Andres Formation was constructed based on our updated top of San Andres picks (Figure 2.4). This trend residual map was introduced in the November 2006 Semiannual Scientific/Technical Report and is calculated by subtracting the calculated 4th-order trend from the configuration map of the top of the San Andres Formation. Positive residuals correspond to locations where the configuration surface lies above the trend surface. The 4th-order trend surface residual map delineates dominant NW and NE lineaments on the surface that reflect, in part, 1) structural deformation associated with the southeasterly

plunging anticline that crosses the area, 2) a secondary northeasterly structural trend that may have preceded the anticline, and 3) erosional topography possibly related to the karst development.

Results of the statistical petrophysical analyses to characterize the karst at the top of the San Andres Formation, described in the previous section, are summarized in maps, including: 1) thickness of tight (non porous) interval at the top of the San Andres Formation (Figure 2.5) and 2) thickness of the anhydrite-dominated zone in the upper San Andres Formation (Figure 2.6). The thickness of the tight zone is notably less in the northern portion of the map corresponding to the north flank of the structure and an area with negative 4th-order residuals (Figures 2.1 and 2.4). The thickness of the anhydritic karst is generally greater on the higher portions of the structure. Further understanding of the karst may come when these maps are correlated with seismic information.

An initial survey of the porous interval that lies beneath the karst was made, using a porosity cutoff of 10%, and the preliminary results are presented in Figures 2.7 and 2.1.8. The depth below the top of San Andres Formation to the top of the porous carbonate with >10% porosity is greatest (~90 ft or 27 m) on the west side of the mapped area and thinnest (<20 ft or 6 m) along a NE-trending zone that corresponds closely with the saddle area on the anticline (seen in Figure 2.4 as a negative 4th order trend residual). Greater depths to the top of porous carbonate with >10% porosity (Figure 2.7) correspond well with moderate thicknesses of tight karst and greater thicknesses of anhydritic karst as defined from petrophysical analyses and statistical zonation (Figures 2.5 and 2.6). All three of these maps show greatest values along the crestal area of the anticline (Figure 2.1). This suggests possible structural control on the karst and the depth to porosity below the karst (i.e., structure may influence the intensity or location of karst development).

The depth from the top of San Andres Formation to the base of the porous carbonate with >10% porosity increases from north (<70 ft or 21 m) to south (>180 ft or 55 m) (Figure 2.8). Greater depths to the base of porosity generally occur over the saddle area of the SE-trending anticline and may indicate the influence of a corresponding paleostructure where the higher shelf realized an earlier (stratigraphically lower) onset of shoal water conditions associated with prominent porosity in the San Andres Formation, e.g., ooid, skeleton grainstones. The wells used in this map fully penetrate the main interval of porous carbonate that lies above the “x” marker described earlier.

A map of the gross porosity thickness, based on the difference between the top and base of the porous carbonate interval with >10% porosity, is shown in Figure 2.9. The porous interval thickens in the south-central portion of the mapped area in the saddle area of the anticline due to: 1) a combination of less karst and stratigraphically higher porosity development and 2) initiation of the porosity at a lower stratigraphic horizon.

A NW-SE structural cross section (C-C’) extending through the mapped area shows the karst as defined by the base of the “tight” zone beneath the top of San Andres (orange-colored line) and the base of the anhydritic section (purple-colored line) (Figure 2.10). The tight zone often extends below the anhydritic section. Karst is recognized as an

interval that is tight without appreciable anhydrite replacement, or it can be both tight and anhydritic. The density porosity (blue-shaded where >10%) and sonic porosity (red-shaded where >10%) logs highlight the porous San Andres Formation that underlies the karst. The gross porous interval in the first 150 feet (46 m) below the top of the San Andres Formation is only a crude first approximation of the reservoir quality. The characterization of the San Andres reservoir will be refined during the next reporting period.

2.2 Seismic Characterization

The "East Ranch" 3-D seismic survey available for the San Andres study area covers a 9 mi x 9 mi (14.5 km x 14.5 km) area, extending well beyond the bounds of the "high volume area" that is the focus of our reservoir study. During this reporting period, we have focused on a 2.5 mi x 3.4 mi (4.1 x 5.4 km) portion of the survey surrounding the "high volume area". Our goal was to develop ties between well data and the 3-D seismic volume and ensure that our seismic interpretations are as accurate as possible in this area. 11 wells in the local study area have both sonic and density logs and an additional 51 wells have sonic logs (Figure 2.11). Synthetic seismograms were constructed for each of these wells and used to tie formation tops to seismic horizons (Figure 2.12).

As mentioned in earlier semi-annual scientific/technical reports, the seismic reflection corresponding to the top of the San Andres Formation is difficult to interpret in the "high volume area". Prior interpretations of the 3-D seismic data have been made using the stacked and migrated amplitude data. In an attempt to improve our interpretations of the top San Andres and other horizons, we have generated a model-based impedance inversion of the seismic amplitude volume in the "high volume area". Our starting model was based on the 11 wells in the area with sonic and density logs. As can be seen in Figure 2.13, the top San Andres is much better defined in the impedance volume than in the original amplitude volume.

A horizon corresponding to the contrast between higher impedance above and lower impedance below that approximates the top of the San Andres Formation has been interpreted across the study area (Figure 2.14). Although this seismic horizon is labeled "San Andres", comparison to tops in wells containing synthetic seismograms indicates that it more closely ties to the base of the tight interval (or the base of the anhydritic karst interval) discussed in Sections 2.1.2 and 2.1.3 (Figure 2.15). This is supported by log data, which show a decrease in impedance at the base of the tight zone but no appreciable impedance contrast associated with the top of the San Andres Formation (See AI log in Figure 2.12).

A new horizon, designated as the "blue" marker, can also be interpreted below the top San Andres and above the Guad 4 regional marker on the impedance volume (Figures 2.15 and 2.16). From well control, this horizon appears to correspond to the "x"-marker discussed in the previous section. The "blue" marker appears to be truncated by the "San Andres" base of karst horizon in the southern portion of the study area and locally in other areas. In the western part of the study area, the "blue" marker is also absent, either

onlapping onto the Guad 4 or having been truncated by the top San Andres unconformity (Figure 2.16).

During the next reporting period, we will quantitatively compare the seismic impedance below the "San Andres" horizon with porosity in the upper San Andres porous interval from log interpretations. We will also attempt to identify if there is a difference in reservoir type/quality in areas where the interval above the "blue" marker/"x" marker is absent.

3.0 MISSISSIPPIAN SPERGEN STUDY AREA

The Mississippian study area is located in Cheyenne Wells and Smoky Creek fields (Fig. 3.1) in Cheyenne County, Colorado, where oil is produced from the Mississippian Spergen reservoir. The Cheyenne Wells and Smoky Creek fields have produced in excess of 8 million barrels of oil since their discovery in 1968; however, well performance in these fields is extremely variable. One of the major motivations behind our study is to explain why adjacent wells show significant variation in oil production.

Geological and petrophysical characterizations of the Cheyenne Wells and Smoky Creek fields were essentially completed during prior reporting periods. These studies suggest that the reservoir comprises three intervals (Spergen A - upper, B - middle, and C - lower). Seismic characterization of the study area, which was initially conducted based on relatively poor quality processed seismic data, was re-evaluated during the present reporting period, based on newly completed re-processing of the seismic data volume.

During the present reporting period, our primary focus has been detailed reservoir modeling for the southern portion of Smoky Creek field. This area was chosen for the focus of our study because most of the wells in this area were drilled in the 1990s and contain modern wireline logs, which are more reliable than the wireline logs from earlier (primarily 1970s vintage) wells for determining reservoir properties such as porosity and water saturation.

3.1 Seismic Characterization

A 5.5 mi^2 (14.2 km^2) 3-D seismic survey covers the central portion of the Cheyenne Wells and Smoky Creek fields (Figure 3.1). Previous semi-annual scientific/technical reports have documented the interpretation and attribute analysis of the seismic data. Because of significant noise in the processed seismic data on which these interpretations were based, the operator recently had the data reprocessed. During the present reporting period, we re-interpreted the horizons of interest and generated new seismic attributes using the reprocessed seismic data.

The reprocessed seismic data volume contains less high-frequency noise than the original processed data volume (Figure 3.2); however, structurally, the new volume is adversely affected by near-surface velocity variations, which produce a time-structure high in the northwest portion of the survey, where well tops indicate a structural low. The near-

surface velocity effects were apparently compensated for in the original processed volume (although the processing parameters used to generate the original processed volume are not known), since the time structure of the original data is a more accurate representation of depth structure (Figure 3.3). Volumetric curvature data generated from the two volumes were also compared, and either the smoother nature of the reprocessed data volume or slight variations in the parameters used to calculate the curvature causes the curvature of the re-processed data to appear rather smeared in comparison to the curvature of the original data (Figure 3.4). Because of these problems with the re-processed data, the decision was made to use the top of Spergen structure map and volumetric curvature derived from the original seismic volume in constructing our reservoir model in Smoky Creek field.

Studies in other areas have indicated that most positive and most negative curvature appear to correlate strongly with fractures (e.g., Blumentritt et al., 2006). Cores from the Cheyenne Wells field show fractures that are mostly filled with chalcedony, megaquartz, and baroque dolomite, rather than being open (May 2006 Semi-Annual Scientific/Technical Report), suggesting that fractures in the Smoky Creek field could serve as barriers to fluid flow, and thus compartmentalize the reservoir. We have plotted most positive curvature and most negative curvature extracted at the approximate level of the top of Spergen along with cumulative oil production from wells in the southern Smoky Creek field (Figure 3.5) and see a general correspondence between wells with lower production and strong positive curvature lineaments. Therefore, in this area, we have chosen the positive curvature to define potential compartment boundaries.

3.2 Smoky Creek Field Engineering Study

Figure 3.6 is an enlargement of the structure map of the Spergen showing the general layout of the Smoky Creek field including well locations. Most of the wells in the middle to southern half of the field are drilled on 40-acre (16-hectare) spacing. Initial drilling commenced in the early 1970s with the majority of the wells being drilled in the early 1990s. Our study aims to explain why adjacent wells show significant variation in oil production. Volumetric curvature analysis of the 3-D seismic data (detailed in the previous section) revealed the existence of possible compartments (Figure 3.7) of varying sizes. Incidentally, barring one compartment, which houses Crosby 1 and Crosby 2 wells, a single well produces from each of the other compartments. The intent of this simulation study was to test whether varying drainage areas, as a result of compartmentalization, contributed to significant production variation between the wells in Smoky Creek field.

3.2.1 Reservoir Pressure, Temperature, API

The initial reservoir pressure was estimated from DSTs run in the wells. Figures 3.8A and 3.8B plot the final shut-in pressures (FSPs) and initial shut-in pressures (ISPs) recorded in DSTs in wells from Smoky Creek and Cheyenne Wells fields. The plotted DST pressures were recorded over different intervals, namely Spergen A, B, and C, or any combination of the above. It is apparent from these two plots that there is a remarkable consistency in pressure in the 3 zones for all the wells, and that the reservoir has undergone minimal pressure decline between 1973 and 1993, thus indicating the presence

of a strong water drive. The initial reservoir pressure was estimated to be 1100 psi (7600 kPa). Well records indicate that measured reservoir temperature varied between 115° to 160°F (46° to 71°C), and that oil API varied between 38 to 41 degrees.

3.2.2 Log Analysis

Suites of modern wireline logs were available from all the wells drilled during the 1990s. Logs from each well were analyzed with PfEFFER software developed by the Kansas Geological Survey using m = n = 2.0 and R_w = 0.08 ohm-m. Cut-off parameters (porosity = 8%, water saturation = 52%, Vshale = 0.45, and BVW = 0.049), that discriminated between dry and productive wells from the Smoky Creek field, were used to delineate effective pay in each well. No cores were available from the Smoky Creek field, and thus, lacking additional petrophysical data, the same cutoffs were applied to Spergen A, B, and C zones. Table 1 lists the thickness, porosity, and S_w of effective pay in Spergen A, B, and C.

3.2.3 Free-Water Level (FWL)

Compilation of the DST recovery descriptions (Table 2) revealed lack of water production when intervals above -1179 feet (-359 m) subsea were tested. Thus, the FWL was initially estimated to be around -1180 feet (-360 m) subsea. The validity of this FWL assumption was tested by plotting log-derived water saturation (S_w) and R_{wa} (apparent resistivity) against depth (Figures 3.9A and 3.9B). As expected, the S_w values hovered between 0.8 and 1.0 and the R_{wa} values stabilized to a narrow band below the estimated FWL of -1180 feet (-360 m) subsea.

3.2.4 Permeability Estimation

Measured rock permeability data are unavailable for the Smoky Creek field, and core data from nearby Cheyenne Wells field exhibited permeability values and permeability-porosity trends that are not consistent with well production histories in the Smoky Creek field. Permeability for effective pay intervals were estimated from published permeability-porosity trends for Mississippian rocks in Kansas. However, there is no assurance that these trends are appropriate for the field nor is there lithologic information necessary to know which of several lithologically-specific permeability-porosity relationships to use. To predict permeability, the wireline-log calculated S_w and assumed capillary pressure (P_c) relations that relate S_w and permeability were utilized. Using generalized capillary pressure curves for Mississippian rocks, Byrnes and Bhattacharya (2006) have shown that S_w at any given height above FWL is related to capillary pressure using the following relation:

$$S_w = \left[\frac{[Bh(\rho_w - \rho_o]}{\frac{P_{ce}}{100^{Pcf}}} \right]^{1/Pcf}$$

where B is a proportionality constant (= 0.433 psi cc/ft g), h is the oil column height (ft), ρ_w and ρ_o are the water and oil specific gravity (g/cc), P_{ce} is the oil-water capillary threshold entry pressure (psi), P_{cf} is the dimensionless measure of pore size heterogeneity, and S_w is the water saturation at height, h. In this equation P_{ce} and P_{cf} have been empirically related to permeability (k) for Mississippian rocks using the following relationships:

$P_{ce} = 2.30\ k^{-0.42}$
$P_{cf} = 0.168\ \ln(k) - 1.985$

To predict permeability, S_w at each half-foot interval was calculated from wireline log response. In addition, from field data the elevation of the FWL was estimated at -1180 feet (-360 m) subsea. The elevation above the FWL for each half-foot of the effective pay was calculated (h). Inserting the P_{ce} and P_{cf} equations into the S_w equation and solving for permeability it is possible to predict permeability given S_w and height above FWL (h).

Figure 3.10 crossplots calculated permeability versus log-calculated porosity. This permeability-porosity trend is consistent with trends exhibited by Mississippian rocks on the Central Kansas Uplift by packstone lithology (blue line), packstone-grainstone lithology rocks (red line), and packstone-wackestone lithology rocks (green line). In general, using this methodology, permeability was predicted every half-foot within each well's effective pay interval in the Smoky Creek field. Predicted permeabilities for a well interval were generally within 50% of the mean permeability for the interval.

3.2.5 Production Performance

Table 1 lists the recovery efficiencies (REs) of wells from the Smoky Creek field assuming that each well drained 40-acres (16 hectares). The majority of the wells show a RE less than 50%. However, 3 wells show unrealistically high RE values, confirming the concerns of the field operator, i.e., significant variation in productivity between nearby wells. Figure 3.11A shows plots of water-oil-ratios (WORs) versus time for wells from the Smoky Creek field with the Crosby 4 data scaled to the secondary (right) Y-axis. A closer look (Figure 3.11B) at Crosby 1 and Kern 1 data show that the WORs for these two wells almost overlap until 1993, after which the water production from the Kern 1 well shows a steep and sudden increase. Well records show a pump change in 1994 at Kern 1, and the operator suspects higher water cuts as a result of the larger pump put in place. Figure 3.11C plots the WOR data for the other wells and it is apparent that Crosby 4 (scaled to secondary Y-axis) and Hiss 2 show high water cuts. Figure 3.11D compares WORs from Crosby 4 and Hiss 2, and it shows that the water cuts from these 2 wells traced each other until 2001, and thereafter Crosby 4 showed a sudden and significant increase in water production to a level that proved uneconomic for operation of this well in September 2003. Again, well records indicate a pump change in May 2001, and the operator suspects that installation of a larger pump resulted in significant increase in water production. The WOR plots indicate the following: a) continuous increase in WOR with time at all wells, suggestive of a strong water drive; b) differences in WOR profiles between wells; and c) very high WORs recorded at a few wells are probably due to

mechanical reasons such as installation of large pump units rather than due to reservoir driven causes.

3.2.6 Reservoir Simulation

Previously discussed volumetric curvature analyses of 3-D seismic data from Smoky Creek field reveal possible compartmentalization of the reservoir. Also, the REs at some of the wells are unrealistically high assuming 40-acre (16-hectare) drainage areas. One possible explanation for uneven production from adjacent wells is varying sizes of drainage compartments. To test this hypothesis, one of the larger compartments, marked in red on Figure 3.7, was simulated. This compartment is the only compartment delineated in the Smoky Creek field that appears to house two wells, namely, Crosby 1 and Crosby 2. Figures 3.12A and 3.12B plot the oil and water production along with the WORs for these two wells.

Table 3 summarizes some of the important input parameters for the reservoir and the aquifer system used during simulation studies of the above mentioned compartment in the Smoky Creek field. Geologic studies, detailed in previous reports, reveal that the Spergen interval in Smoky Creek field comprises three layers, i.e., A, B, and C. Log analysis and perforation histories show that the primary production interval in this field is the Spergen A layer which is present in all the wells. Some of the wells show additional effective pay in Spergen B and/or C. Thus, the reservoir modeled in this study comprised 3 layers using 100 feet by 100 feet (30 m by 30 m) grid cells.

Based on the reconciliation of log-S_w and P_c, the permeability estimated in the Spergen effective pay varied between 20 to 40 md. However, permeability multipliers had to be used to bring the permeability in the range of 75 to 110 md in order to match the cumulative oil and water production at Crosby 1 and 2 wells (Figures 3.13 and 3.14). Four day static buildup tests were carried out at both these wells in 2001 revealing a reservoir pressure close to 1000 psi (6900 kPa). Also, flowing bottom hole pressures (FBHPs) of 475 psi (3275 kPa) (as of Sep 2001) and 461 psi (3180 kPa) (as of Sep 2005) were recorded at Crosby 2 while a FBHP of 543 psi (3745 kPa) (as of May 2004) was measured at Crosby 1. Figure 3.15 shows that the simulator calculated average reservoir pressure was slightly less than 1000 psi (6900 kPa) while FBHPs at Crosby 1 and 2 hovered around 600 psi (4140 kPa). Thus, when permeability values in the Spergen layers varied between 75 to 110 md, a reasonable history match was attained for Crosby 1 and 2 wells assuming that they produced from a single compartment as demarked in Figure 3.7.

3.2.7 Future Studies

The average porosity in the most productive parts of the effective pay is close to 12 percent which results in an estimated permeability between 30 and 40 md (Figure 3.10). However, if the formation porosity was 2 (percent) units higher, say 14 percent, then the estimated permeability in the best parts of the effective pay would be between 60 to 80 md – a range close to that required to obtain performance history matches. A comparison of core porosity to log porosity in the cored Klepper #4 well in Cheyenne Wells field does show a discrepancy between the core and log porosity measures in the vicinity of

the perforated interval, with the core porosity higher than the log porosity by up to 5 porosity units (May 2006 Semi-Annual Scientific/Technical Report). This suggests that a 2 porosity unit discrepancy in the log porosity for Smoky Creek field is not unreasonable.

One course of action for future studies would be to confirm if the wireline logs were underestimating the formation porosity in Smoky Creek field. Another obvious course of action will be to simulate all the compartments with wells (in Figure 3.7) to confirm if the compartments delineated from volumetric curvature analyses are realistic, and if such compartmentalization could explain the wide differences in productivity between the wells.

The volumetric curvature map in Figure 3.7 suggests that there are potentially untapped compartments in Smoky Creek Field. Depending upon the reservoir properties, these may be potential drilling targets. If simulation of the curvature-delineated compartments containing wells is successful, we will also model the potential for additional resources in the untapped compartments, assuming reservoir properties similar to those in surrounding wells.

4.0 Arbuckle Study Area

The Arbuckle study area, in Russell County, Kansas, is a 9 mi^2 (23 km^2) area covered by a 3-D seismic survey (Figure 4.1). In this study area, the Arbuckle reservoir sits at or near a pre-Pennsylvanian unconformity and karst surface, and Arbuckle production is located on local remnant highs. Our previous work has described the regional geological setting of the Arbuckle study area and has suggested that the seismic survey is in an area of polygonal karst. Fields in areas of polygonal karst tend to be relatively small and irregularly shaped, often with relatively low individual well production (Cansler and Carr, 2001). The goal of our present work has been to begin detailed reservoir characterization of the Arbuckle within the seismic survey area.

4.1 Data Availability

Because Arbuckle reservoirs in Kansas have been traditionally modeled as an oil column on top of a strong aquifer, Arbuckle wells historically have been drilled into the top of the Arbuckle with relatively shallow penetration (rarely > 10 ft (3 m)) and open-hole completion (Franseen et al., 2004). Most of the wells within our study area are typical of these practices. While 28 wells within the seismic survey area contain porosity, resistivity, and gamma ray logs necessary for determining the critical input petrophysical parameters for a reservoir model, less than half of those wells penetrate more than a dozen feet (4 m) into the Arbuckle. Also, for most of the wells, porosity is derived from the neutron log only and resistivity is from the guard log. Only 8 wells have density-neutron porosity, which allows for better lithology-independent porosity estimations than neutron porosity alone, and deep laterolog resistivity, which is less sensitive to invasion than the shallow guard log.

31 wells within the seismic survey area produce from the Arbuckle (Figure 4.1). However, a number of these wells are completed in multiple intervals and production is commingled. Also, since only lease production is available for the study area, even wells that produce solely from the Arbuckle are often in the same lease as an adjacent well or wells producing from a different interval.

The lack of reliable production data, along with the scarcity of log data may preclude us from conducting a comprehensive reservoir simulation for the Arbuckle study area. However, we are still investigating methods for assigning lease production to individual wells and for estimating reservoir properties in wells with inadequate logs. We begin by conducting a detailed characterization of the Arbuckle for the 8 wells with neutron, density, and deep laterolog logs.

4.2 Oil/Water Contact

Wireline logs have been used to estimate the depth to the oil/water contact across the survey area. We have defined the oil/water contact from logs as the depth below which the apparent resistivity (R_{wa}) stabilizes and water saturation (S_w) hovers near 1. This depth also corresponds to the depth where BVW and porosity begin to track one another (Figure 4.2). The height of the oil/water contact from log analysis varies from -1482 to -1506 ft (-451 to -459 m) subsea within the study area (Figure 4.1). Where there is not sufficient log data to determine the oil/water contact from log analysis, reported oil/water contacts from ACO-1 forms have been used.

The variation in oil/water contact within the study area is most likely due to the fact that the Arbuckle subcrop is changing across the study area, with associated variation in petrophysical properties.

4.3 Arbuckle Subcrop Characterization

Pickett plots have been constructed in PfEFFER for the wells for which top of Arbuckle appears to be above the oil/water contact and that also contain neutron, density, and deep laterolog logs. The Pickett plots are shown for three of these wells in Figure 4.3. Wells #1 and #2 are within the same local structural high (Figure 4.1) although the top of the Arbuckle is approximately 20 ft (6 m) lower in well #2 than in well #1. The top of Arbuckle is at approximately the same subsea depth in wells #1 and #3, although they are in different structural highs, separated by approximately 2 miles (3 km).

The Pickett plots and a well log cross section (Figure 4.4) highlight variability in the porosity distribution of the Arbuckle subjacent to the pre-Pennsylvanian unconformity surface. Wells #1 and #2, located approximately 0.5 mile (0.8 km) apart, are relatively similar, both exhibiting coarsening upward trends, as indicated by decreasing resistivity with increasing porosity along a constant water saturation line as depth increases. In addition to an upward decrease in BVW consistent with an upward increase in pore size, these wells also appear to show the same irreducible BVW, approximately 0.068. However, there is a difference in reservoir quality, with well #2 showing poorer, lower

porosity (~8% vs. 12%) reservoir above the oil/water contact, in addition to being structurally lower than well #1. Well #2 is a dry hole, while well #1 was completed in the Arbuckle; however, well #1 only produced for 15 years from multi-pay zones, thus is considered a marginal well. This performance is consistent with a relatively high water saturation (>60%).

The Pickett plot for well #3 is quite different than plots for wells #1 and #2. Well #3 exhibits a tight zone at the top of the Arbuckle characterized by high BVW indicative of small pore size. This zone falls below the 100% water saturation line, suggesting changes in pore architecture requiring different Archie parameters, m and n, than used here. The tight zone is underlain by a relatively uniform layer where points tightly cluster near constant porosity (9-12%) and water saturation as low as 45%, with an irreducible BVW of approximately 0.055. BVW and water saturation are the lowest of the three wells, suggesting larger pores, indicating better reservoir quality and greater oil saturation. However, this well was not completed in the Arbuckle.

Future work will attempt to tie the spatial variations in Arbuckle reservoir properties with seismic attributes, including impedance and volumetric curvature.

5.0 BEST PRACTICES WORKFLOW

Although the efficacy of any given seismic attribute for use in reservoir characterization is site specific with regard to geology, seismic acquisition parameters, and image resolution, we have assembled a generalized workflow (Fig. 5.1) for interpreting select seismic attribute data (particularly geometric attributes) and incorporating the results into construction of a reservoir geomodel in reservoirs affected by karst. Our interpretation workflow is based on seismic experience with a variety of karst types and has been largely developed from work in the three study areas in this project, as well as Mississippian Spergen reservoirs in Kansas (e.g., Nissen et al., 2004) and an Ordovician Ellenburger aquifer in the Fort Worth Basin, north Texas (Sullivan et al., 2006).

Effective application of geometric seismic attributes begins with proper pre-processing. We use conventional P-wave 3D seismic data, acquired and processed by individual petroleum companies through commercial vendors. For each poststack volume, we apply edge preserving principal component filtering to suppress random noise and to enhance subtle discontinuities and offsets at minor faults. Next, we calculate a complete suite of geometric seismic attribute volumes on both the original and edge-enhanced seismic data.

For our interpretational workflow, we begin with tying logs to seismic through synthetic seismograms, and then map structure and karst surface geomorphology. Seismic expression of karst geomorphologies may contain subtle, low contrast, features or highly irregular features associated with surface erosion and cavern collapse. Features that are too irregular to be reliably mapped by an interpreter can be observed using time slices or stratal slices, parallel to a nearby interpreted horizon, from coherence or curvature volumes. For more gently eroded landscapes, we can extract data directly along an interpreter-picked horizon. Features that are too subtle to be seen on horizon time

structure and coherence maps, such as small-offset faults or joint-related lineaments, can be imaged with curvature extractions. In areas where the horizon of interest is difficult to interpret using the original seismic amplitude volume, impedance inversion has the potential to improve image resolution.

Information from the horizon structure, and from coherence and curvature volumes, is integrated with geologic data to classify the type of karst overprint and to predict the effect on reservoir performance of the observed features. This methodology can provide insight on origin of observed features and may help identify uncertainties in reservoir quality, compartmentalization, and seal integrity. In areas where reservoir properties, such as porosity, are relatively constant over a great enough vertical extent to be accurately defined by seismic, impedance information can be used to help quantify lateral porosity distribution for reservoir geomodels.

6.0 TECHNOLOGY TRANSFER

The following publications were released during the October 1, 2006, to March 31, 2007, reporting period:

Givens, N. B., 2006, An integrated study delineating karst and fracture features affecting reservoir performance in a Mississippian reservoir, Cheyenne County, Colorado, Master's Thesis, The University of Kansas, Lawrence, 570 p.

Nissen, S. E., T. R. Carr, and K. J. Marfurt, 2007, Using new 3-D seismic attributes to identify subtle fracture trends in Mid-Continent Mississippian carbonate reservoirs, RMAG-DGS 13th Annual 3-D Seismic Symposium expanded abstract (also published in Geophysical Society of Kansas May-June newsletter: http://gsks.seg.org/newsletter/MAY-JUN07.pdf)

Rocke, B. J., 2006, Paleokarst morphologies of the Arbuckle Group and karst reservoir implications on the Central Kansas uplift, Russell and Barton Counties, Kansas, Master's Thesis, The University of Kansas, Lawrence, 210 p.

Sullivan, C., S. Nissen, and K. Marfurt, 2006, Application of volumetric 3-D seismic attributes to reservoir characterization of karst-modified reservoirs, in Slatt, R. M. et al., Eds., Reservoir Characterization: Integrating technology and business practices, 26th Annual GCSSEPM Foundation Bob F. Perkins Research Conference Proceedings, p. 409-428.

The following abstracts have been accepted for presentation at the 2007 Midcontinent AAPG meeting:

Carr, T. R., and S. E. Nissen, Application of curvature attributes to Kansas subsurface data.

Nissen, S. E., E. C. Sullivan, K. J. Marfurt, and T. R. Carr, Improving reservoir characterization of karst-modified reservoirs with 3-D geometric seismic attributes.

In addition, information related to the project (including project background, personnel, a catalog of seismic karst features, publications, and semi-annual scientific/technical reports) is posted to our project website: http://www.kgs.ku.edu/SEISKARST.

7.0 CONCLUSIONS

General

Results of our study to date indicate that 3-D seismic data has enhanced interpretations of the reservoir within all study areas. In particular, volumetric curvature attributes and impedance inversion have revealed previously unknown features in the seismic data and provided enhanced visibility of karst and fracture features. Volumetric attribute horizon and time slices are useful for interpreting features relating to structure (e.g., faults, folds), geomorphology (e.g., sinkholes, polygonal karst), and reservoir architecture (e.g., compartment boundaries). Our best practices workflow suggests that integrating geologic data with information from seismic horizon structure and volumetric attributes allows us to classify the type of karst overprint (e.g., polygonal karst vs. groundwater-sapped plateaus) and to distinguish tectonic features from karst features. This methodology can provide insight on origin of observed features and may help identify uncertainties in reservoir quality, compartmentalization, and seal integrity.

San Andres study area

- Karst within the upper San Andres Formation in the "high volume area" can be separated into 1) "macro" karst, which is predominantly non-porous and is characterized by intense chaotic brecciation and anhydrite replacement, and 2) "micro" karst, where matrix properties dominate fluid flow. The "micro" karst is included as part of the *in situ* bedded carbonate reservoir of the San Andres Formation.
- The base of the tight, anhydritic "macro" karst is interpreted from wireline logs using a statistical zonation program. Porosity is obtained from the sonic log and the anhydrite content is estimated from the density, neutron porosity, and photoelectric factor curves.
- The base of the karst can be interpreted from a seismic impedance volume as a horizon separating high impedance (tight karst zone) above from lower impedance (porous reservoir interval) below.
- The karst zone exhibits high variability in thickness but is generally thicker on the higher portions of the SE-trending anticline that runs through the "high volume area".
- The porous carbonate reservoir interval below the karst is thickest on the saddle area of the SE-trending anticline. Also, depth to the base of porous carbonate is greater along this saddle area of the structure, suggesting a structural influence.
- A seismic horizon corresponding roughly to the base of the porous reservoir, can be interpreted across the impedance volume. This horizon is truncated by the base of karst in some areas, suggesting that there may be an associated change in reservoir type/quality in these areas.

Mississippian study area

- Spergen production in Smoky Creek field cannot be explained using standard log analysis and 40-acre (16 hectare) drainage.
- Most positive curvature extracted along the approximate top of Spergen reveals several potential reservoir compartments.
- Initial results of reservoir simulation of one of the curvature-defined compartments show reasonable history matches of both production and pressure for the two wells modeled.

Arbuckle study area

- The depth to the oil/water contact varies by up to 25 ft (8 m) between structural compartments within the study area, suggesting variation in the petrophysical properties of the uppermost Arbuckle across the study area.
- Pickett plots confirm lateral variation in the Arbuckle reservoir properties between compartments, but also show that there are variations in reservoir quality within a single compartment.

LIST OF TABLES

LIST OF FIGURES

REFERENCES

Blumentritt, C. H., Marfurt, K. J., and Sullivan, E. C., 2006, Volume based curvature computations illuminate fracture orientations – Early to mid Paleozoic, Central Basin Platform, West Texas: Geophysics, v. 71, no. 5, p. B159-B166.

Bohling, G.C., Doveton, J.H., Guy, W., Watney, W.L., and Bhattacharya, S., 1998, PfEFFER 2.0 manual, Kansas Geological Survey, Lawrence, Kansas, 161 pp.

Byrnes, A.P., and Bhattacharya, S., 2006, Influence of Initial and Residual Oil Saturation and Relative Permeability on Recovery from Transition Zone Reservoirs in Shallow-Shelf Carbonates, SPE 99763, 2006 SPE/DOE Symposium on Improved Oil Recovery, Tulsa, Oklahoma, April 22-26, 2006, 11 pgs.

Cansler, J. R., and T. R. Carr, 2001, Paleogeomorphology of the Sub-Pennsylvanian Unconformity of the Arbuckle Group (Cambrian-Lower Ordovician): Kansas Geological Survey, Open-file Report 2001-55, http://www.kgs.ku.edu/PRS/publication/OFR2001-55, accessed June 2007.

Franseen, E. K., Byrnes, A. H., Cansler, J. R., Steinhauff, D. M., and Carr, T. R., 2004, The geology of Kansas -- Arbuckle Group, *in* Current Research in Earth Sciences, Kansas Geological Survey, Bulletin 250, part 2. http://www.kgs.ku.edu/Current/2004/franseen/franseen1.html, accessed June 2007.

French, V. L., and C. Kerans, 2004, Accommodation-controlled systems-tract-specific facies partitioning and resulting geometric development of reservoir grainstone ramp-crest shoal bodies, in Integration of outcrop and modern analogs in reservoir modeling: AAPG Memoir 80, p. 171-190.

Holz, M.H., Jackson, J.A., Jackson, K.G., and Major, R.P., 2002, Petrophysical characterization of Permian shallow-water dolostone: SPE 75214, 16 pp.

Nissen, S. E., Marfurt, K. J., and Carr, T. R., 2004, Identifying subtle fracture trends in the Mississippian saline aquifer unit using new 3-D seismic attributes: Kansas Geological Survey Open-File Report 2004-56. http://www.kgs.ku.edu/PRS/publication/2004/2004-56/, accessed June 2007.

Sullivan, E. C., Marfurt, K. J., Lacazette, A, and Ammerman, M., 2006, Application of new seismic attributes to collapse chimneys in the Fort Worth Basin: Geophysics, v. 71, no. 4, p. B111-B119.

Table 1. List of thickness, porosity, and S_w of effective pay in Spergen A, B, and C at Smoky Creek wells.

		1st Prod		MBO	MBW										Pfeffer	
		Completion		Cum	Cum	Spr A ----------			Spr B ----------			Spr C ----------			MBO	
UWI	Well Name	DATE	Elev	Oil	Wtr	H, ft	Phi	Sw	H, ft	Phi	Sw	H, ft	Phi	Sw	HC Vol	RE, %
15-017-06138	Champlin Kern 1	12/13/1973	4241	1.9	363.4											
15-017-06143	Kern A1	3/22/1974	4249	333.5	381.6											
		3/22/1974														
15-017-06133	Crosby 1	5/29/1973	4215	255.2	1950.6	2	0.11	0.36	2	0.12	0.39	2.5	0.12	0.4	142.9	178.6
05-017-06134	Kern 1	6/28/1973	4229	74	1067.1	5.5	0.122	0.38	1.5	0.131	0.338				163.4	45.3
15-017-07409	Mull UPRC-HISS 2	7/6/1994	4259	80.9	1365.8	8	0.11	0.36							166.6	48.6
15-017-07395	Mull UPRC-HISS 1-X	10/6/1993	4227	228	938.2	15.5	0.134	0.153	3	0.087	0.49				561.5	40.6
05-017-07392	Crosby 4	9/16/1993	4241	64.2	1105.5	8.5	0.117	0.393							178.5	36.0
05-017-07376	Crosby 3	8/4/1993	4209	209	216.2	9	0.133	0.278							255.6	81.8
05-017-07337	Crosby 2	12/8/1992	4257	97.8	888.4	13.5	0.122	0.236	9	0.109	0.35	6	0.092	0.486	658.1	14.9
05-017-07293	Kern A4	2/26/1992	4258	85.8	99.9	9.5	0.087	0.305							169.9	50.5
05-017-07292	Kern 3	3/27/1992	4193	101.2	272.3	7	0.096	0.364	8	0.131	0.288				358.1	28.3
05-017-07239	Kern 2	9/25/1991	4223	173.6	282.4	2.5	0.096	0.416	7	0.152	0.274				281.3	61.7

Table 2. Compilation of the DST recovery from Smoky Creek wells.

		Completion	KB	DST 1	DST 1	Subsea	Subsea	Rec	DST 2	DST 2	Subsea	Subsea	
UWI	Well Name	DATE	Elev	From	To	From	To		From	To	From	To	Rec
15-017-06138	Champlin Kern 1	12/13/1973	4251	5404	5443	-1153	-1192	CO, SMO, FCO, MO, OCRM, OCM, MW					
15-017-06143	Kern A1	3/22/1974	4259	5366	5409	-1107	-1150	SOCM	5405	5440	-1146	-1181	M
		3/22/1974											
15-017-06133	Crosby 1	5/29/1973	4225	5357	5387	-1132	-1162	G, CGO, SMO	5387	5411	-1162	-1186	G, CGO, GOM
		5/29/1973											
05-017-06134	Kern 1	6/28/1973	4239	5347	5390	-1108	-1151	CGO, MGO					
15-017-07409	Mull UPRC-HISS 2	7/6/1994	4271	5404	5450	-1133	-1179	GIP, GMCO, GOCM, OCM					
15-017-07395	Mull UPRC-HISS 1-X	10/6/1993	4239	5345	5415	-1106	-1176	MCO, MCGO, GOCM					
05-017-07392	Crosby 4	9/16/1993	4253	5387	5432	-1134	-1179	GO, SMCGO, HGOCM					
05-017-07376	Crosby 3	8/4/1993	4221	5330	5395	-1109	-1174	GIP, CGO, MCGO, SMCGO, VSOCM					
05-017-07337	Crosby 2	12/8/1992	4269	5385	5450	-1116	-1181	DM, WM, MWWTO					
05-017-07293	Kern A4	2/26/1992	4270	5360	5430	-1090	-1160	CO, HOCM, GOCM, GMCO					
05-017-07292	Kern 3	3/27/1992	4205	5306	5373	-1101	-1168	MCO					
05-017-07239	Kern 2	9/25/1991	4235	5340	5410	-1105	-1175	GIP, CGO, HGCMO					
	No wtr prod when test interval stops at				-1179	subsea							
	Wtr prod when test interval extends to atleast				-1181	subsea							
	Estimated OWC				-1180	subsea							

Table 3. Summary of important input parameters for the reservoir and the aquifer systems for simulation studies.

Reservoir Properties

Rock compressibility	2.00E-06	1/psi	
Ref pressure for rock compressibility	1200	psi	
Reservoir Temperature	135	F	
Oil gravity	40	API	
Water salinity	28,000	ppm	(estimated from Rw = 0.08 ohm-m)

Aquifer definition

Thickness	50
Porosity	0.1
Permeability	100

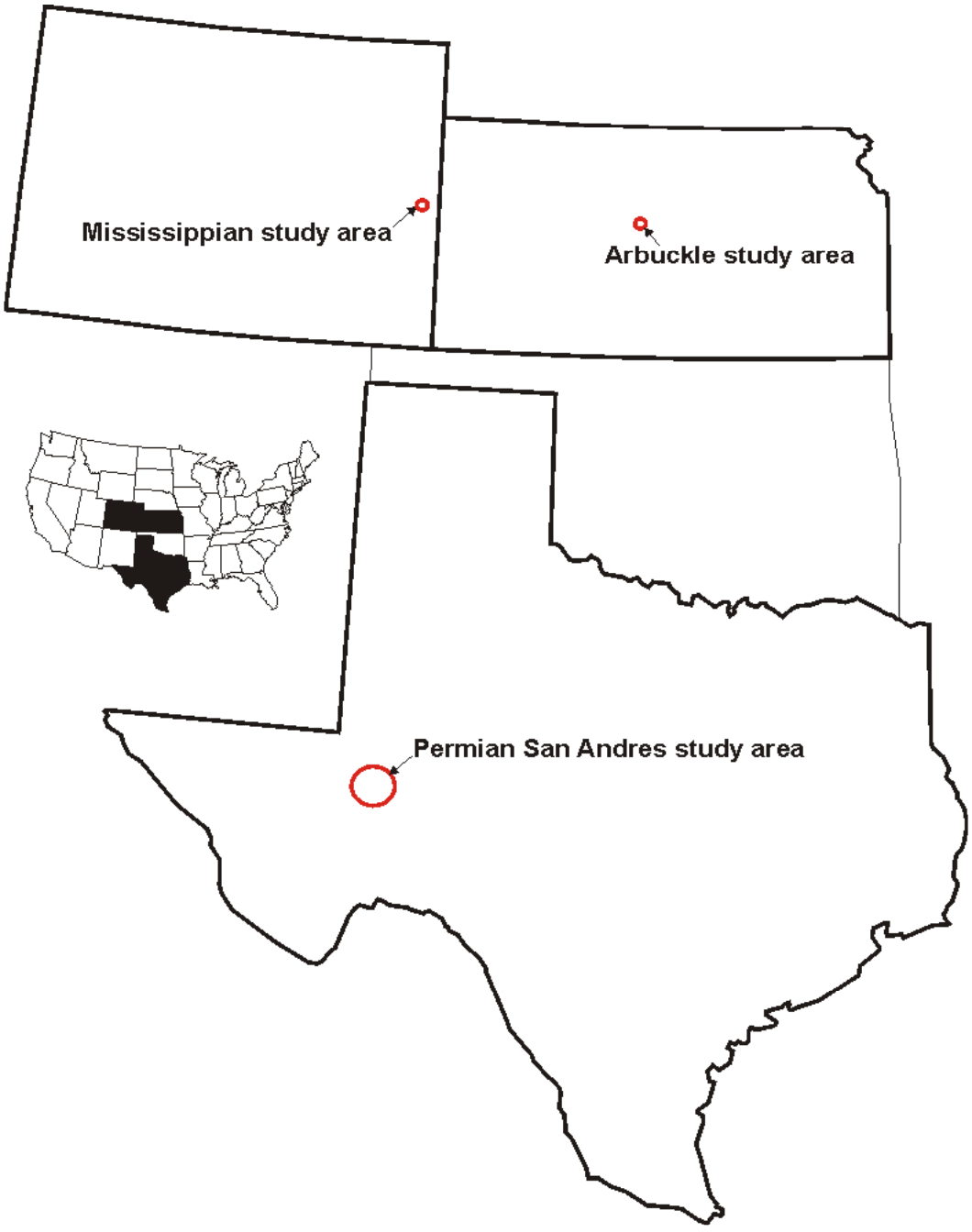

Figure 1.1. Index map showing locations of study areas.

Task Description	Budget Period I										Budget Period II			
	FY05				FY06				FY07		FY08			
	Oct 04	Jan 05	Apr 05	Jul 05	Oct 05	Jan 06	Apr 06	Jul 06	Oct 06	Jan 07	Apr 07	Jul 07	Oct 07	Jan 08
Task 1.0 Obtain 3-D seismic, geologic, petrophysical, and engineering data														
Task 2.0 Generate volumetric attributes														
Task 3.0 Generate preliminary seismic attribute catalog of karst features														
Task 4.0 Perform reservoir characterization studies (seismic, geologic, petrophysical, engineering)														
Task 5.0 Construct integrated 3D reservoir geomodels														
Task 6.0 Conduct reservoir simulations														
Task 7.0 Synthesize best practices workflow														
Task 8.0 Model new well paths														
Task 9.0 Drill, log and core new wells														
Task 10.0 Calibrate attributes and reservoir models with new well data; review and refine attribute-based workflows														
Task 11.0 Rerun reservoir simulations with adjusted parameters														
Task 12.0 Finalize seismic attribute catalog and best practices workflows														
Task 13.0 Technology transfer														

Figure 1.2. Project schedule, revised August 2006.

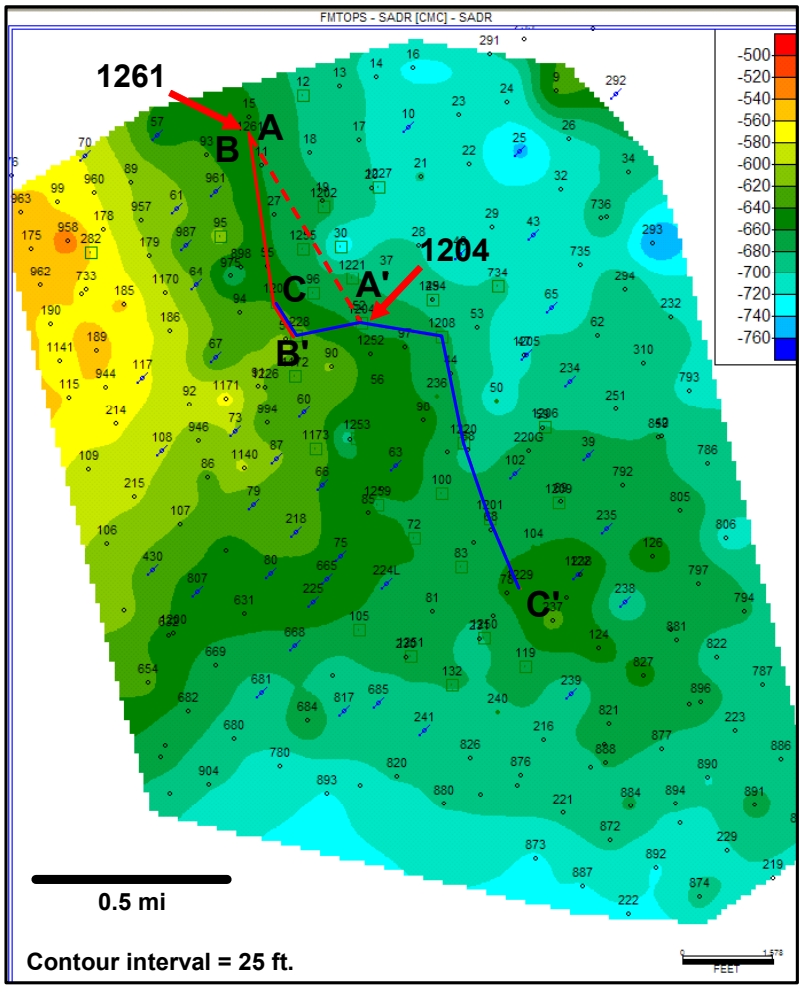

Figure 2.1. Configuration of the top of the San Andres Formation in the "high volume area" of Waddell Field. The map provides index lines locating cross sections shown in Figures 2.2, 2.3, 2.10, and 2.13.

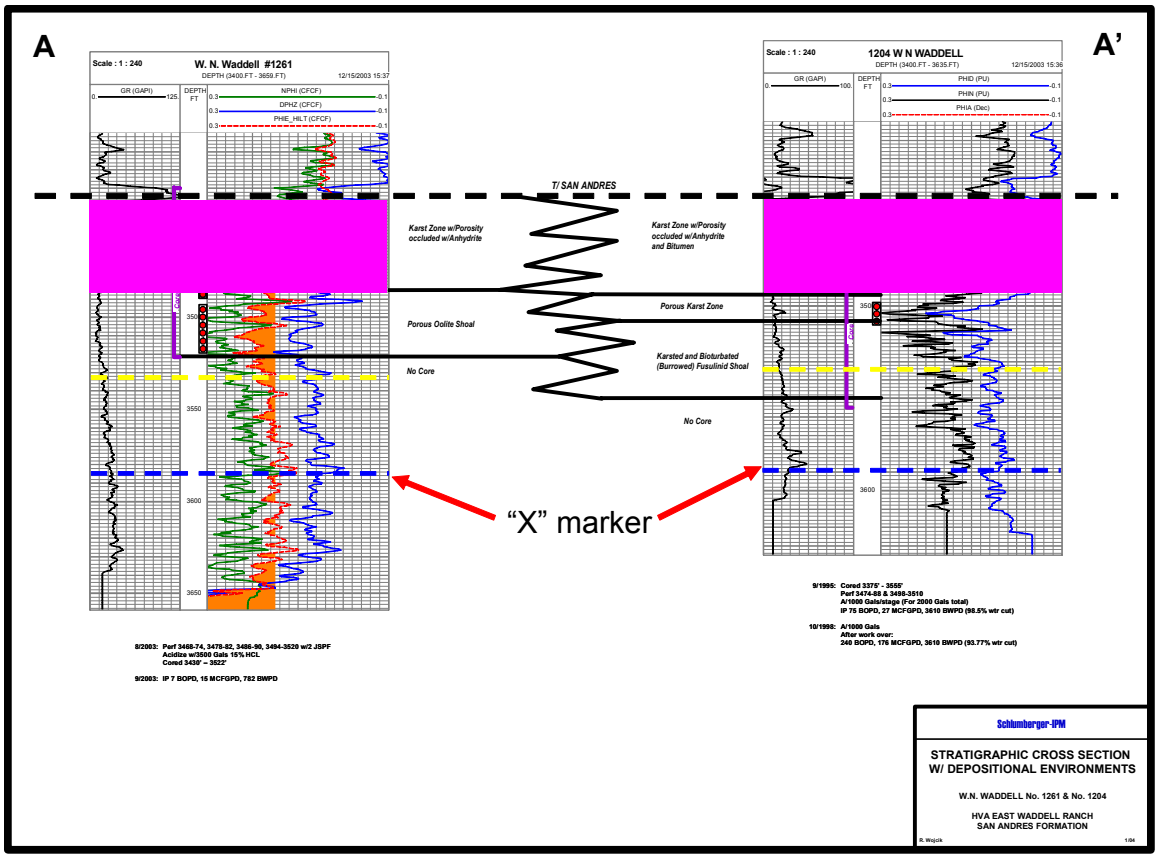

Figure 2.2. Cross section A-A', linking cored wells Waddell #1261 and #1204, modified from a figure provided by the operating company. Modifications include: 1) purple highlighting to identify the intense upper karst typified by low porosity and anhydrite replacement of gypsum, 2) yellow and blue dashed marker horizons. Lower "x" marker consists of a laterally continuous tighter horizon that delimits an upper porosity interval of the San Andres that is perforated for production. Index map is provided in Figure 2.1.

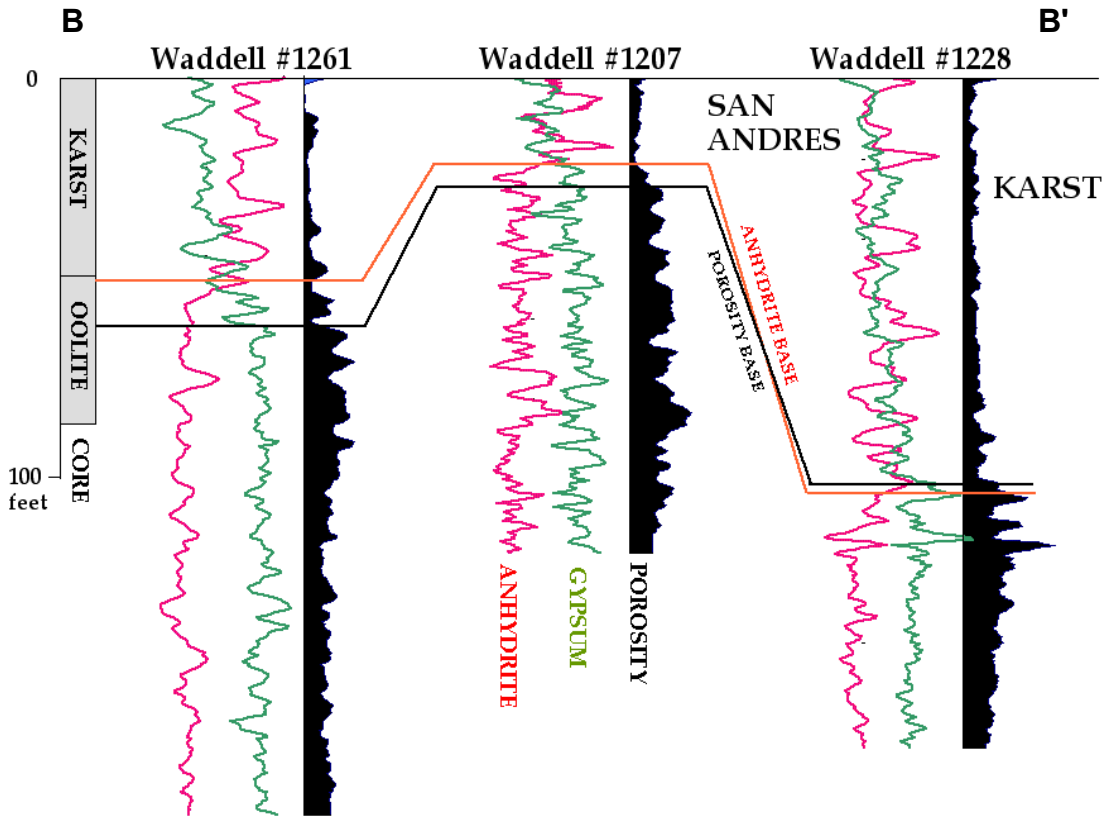

Figure 2.3. Cross-section B-B' from cored well Waddell #1261 through Waddell #1207 and #1228, showing depth profiles of sonic-derived porosity and log-derived estimates of anhydrite and gypsum. Lack of porosity and anhydrite replacement of gypsum are criteria for petrophysical identification of karst developed at the top of the San Andres Formation. Well locations are identified in Figure 2.1.

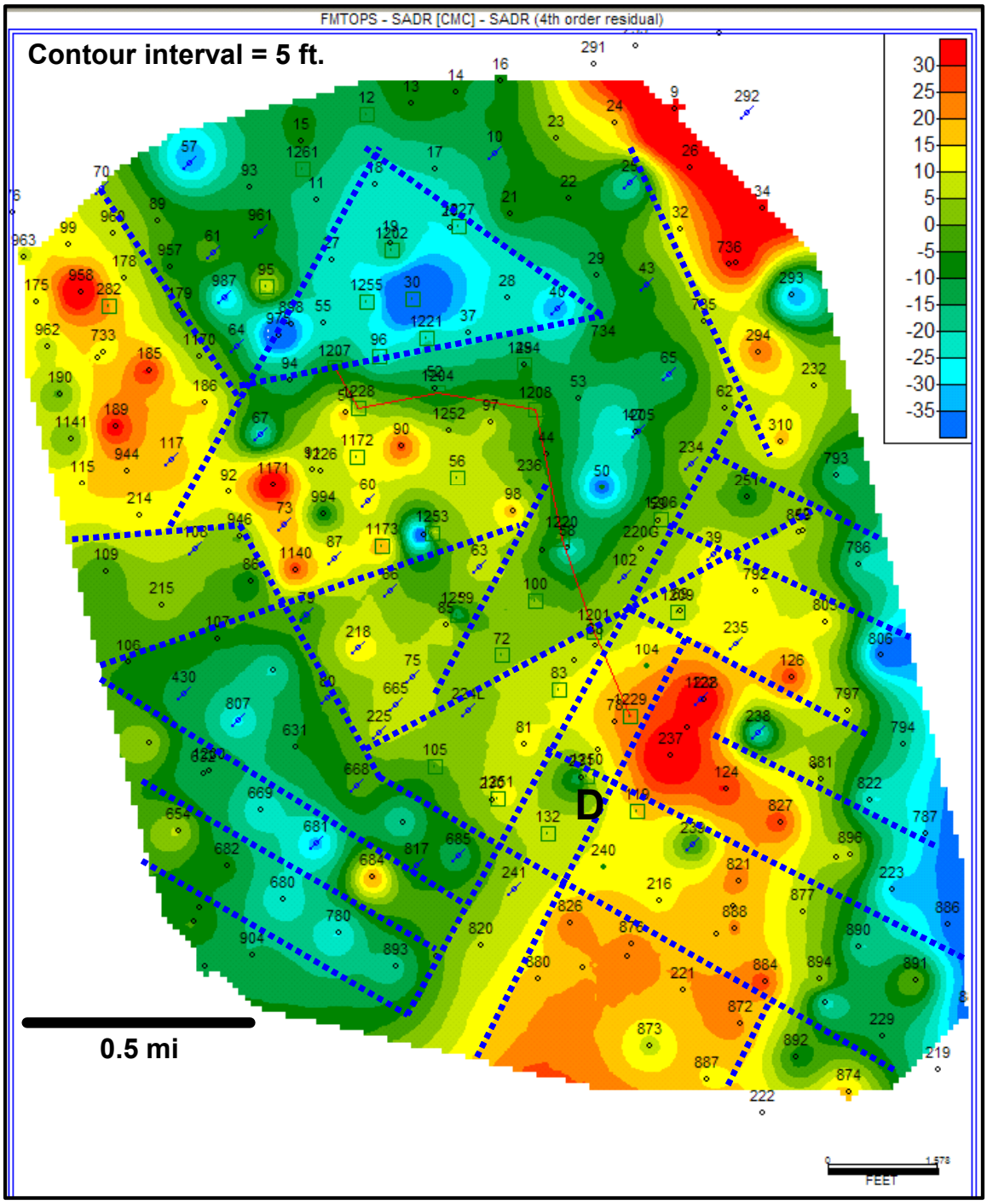

Figure 2.4. Fourth-order trend surface residual of the top of the San Andres Formation. Lineaments (blue dotted lines) are added manually.

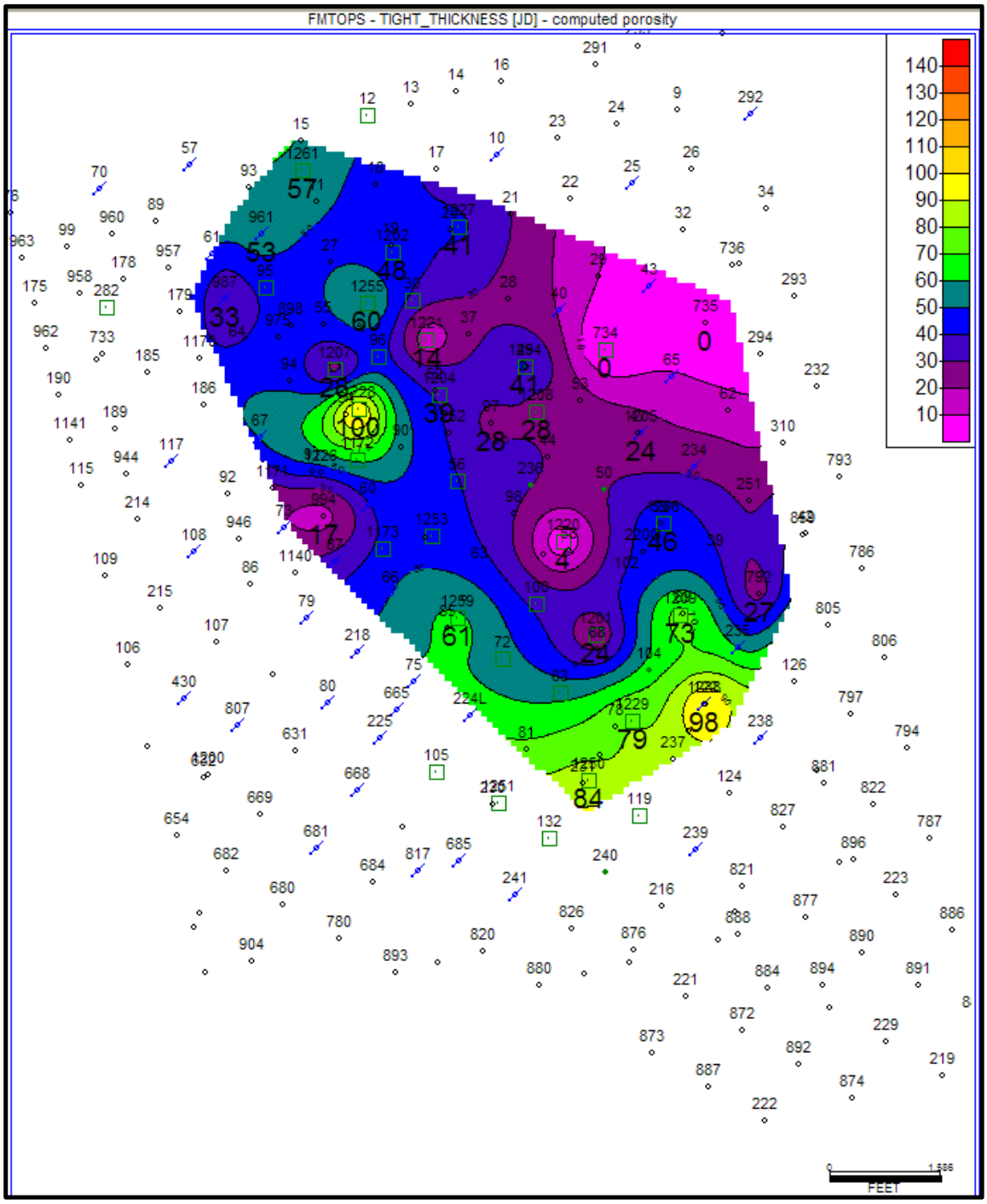

Figure 2.5. Thickness of tight (non porous) interval at the top of the San Andres Formation computed from well logs using a statistical zonation program.

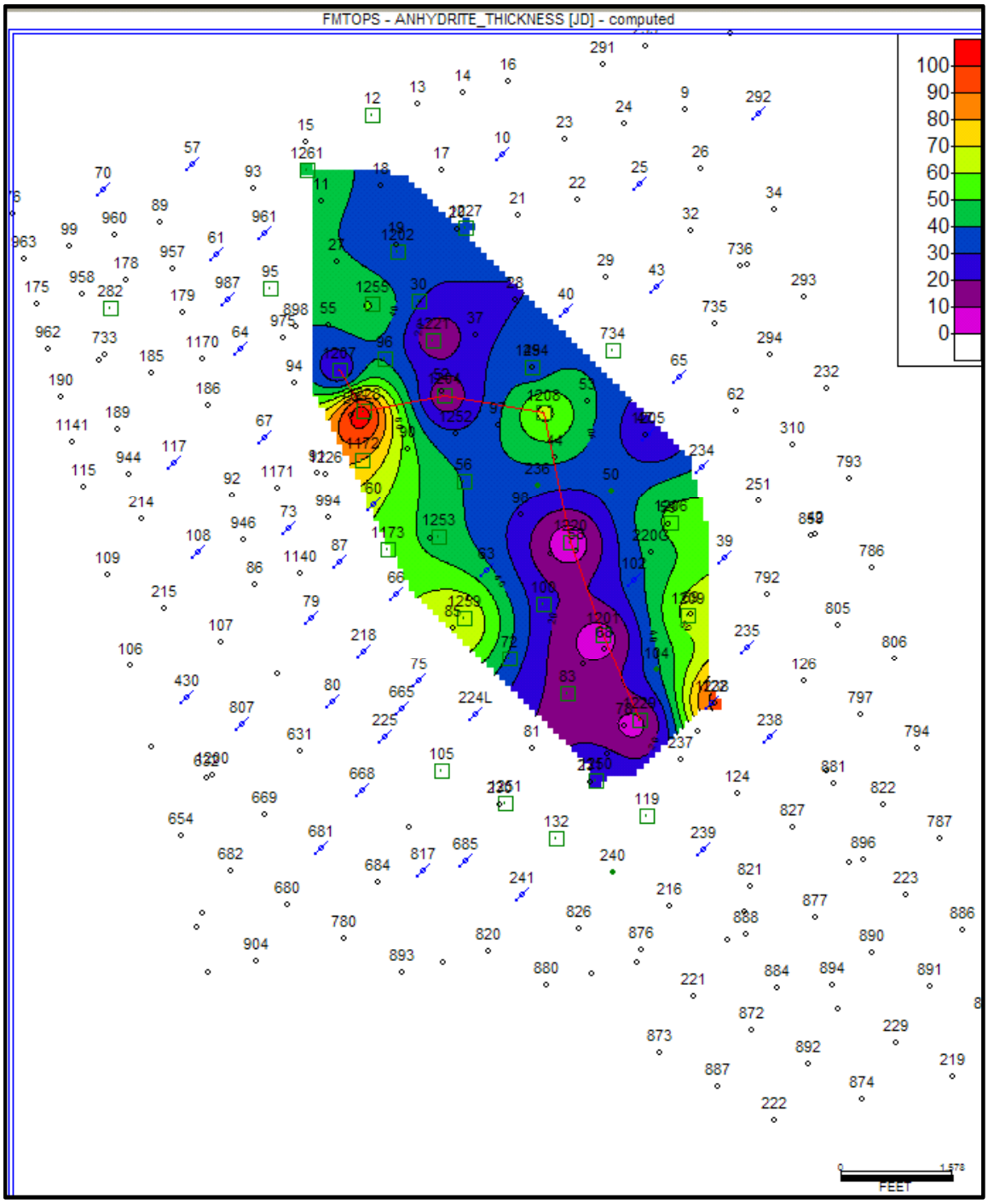

Figure 2.6. Thickness of the anhydrite-dominated zone in the upper San Andres Formation computed from well logs using a statistical zonation program.

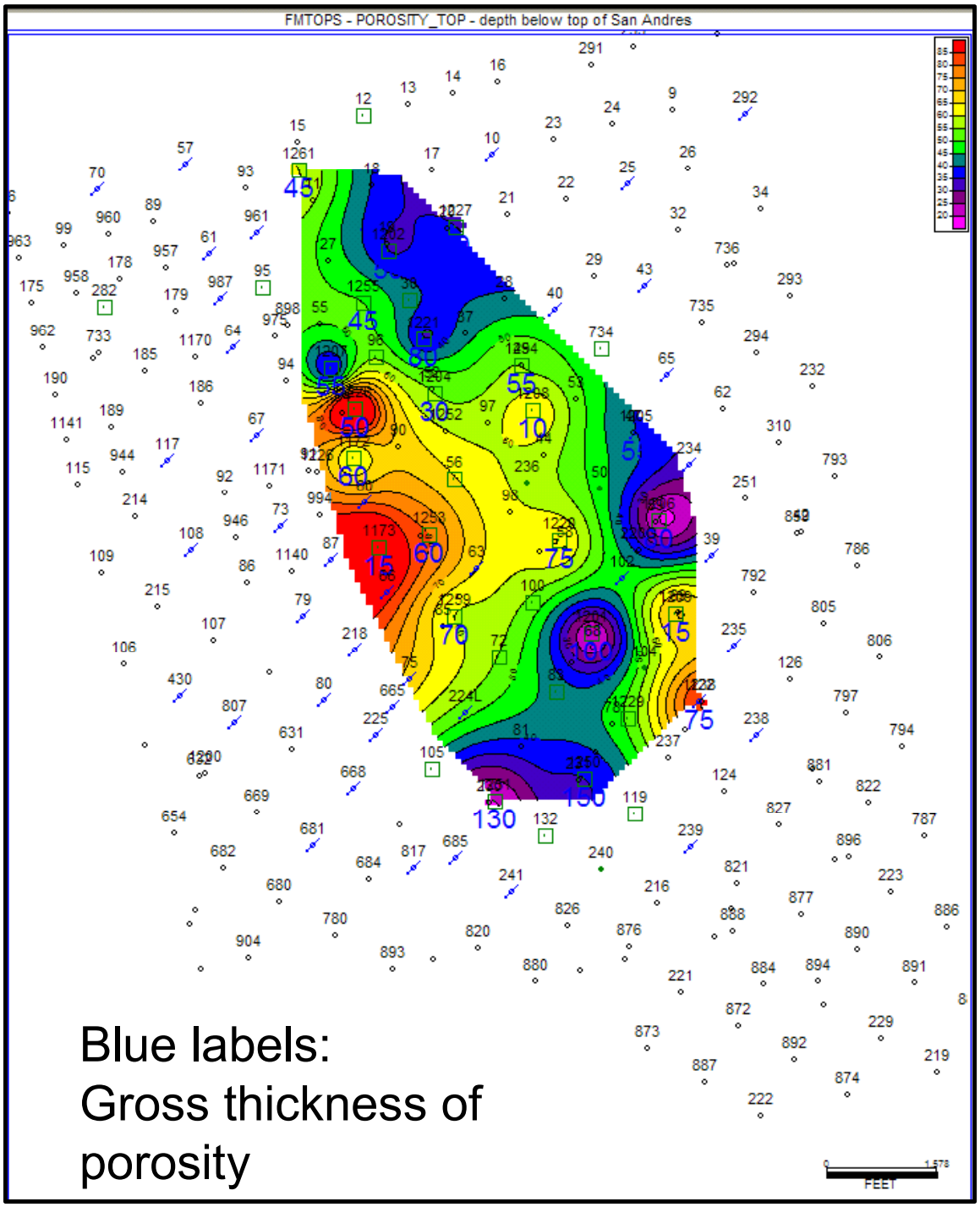

Figure 2.7. Depth below the top of San Andres Formation to the top of the porous carbonate with >10% porosity.

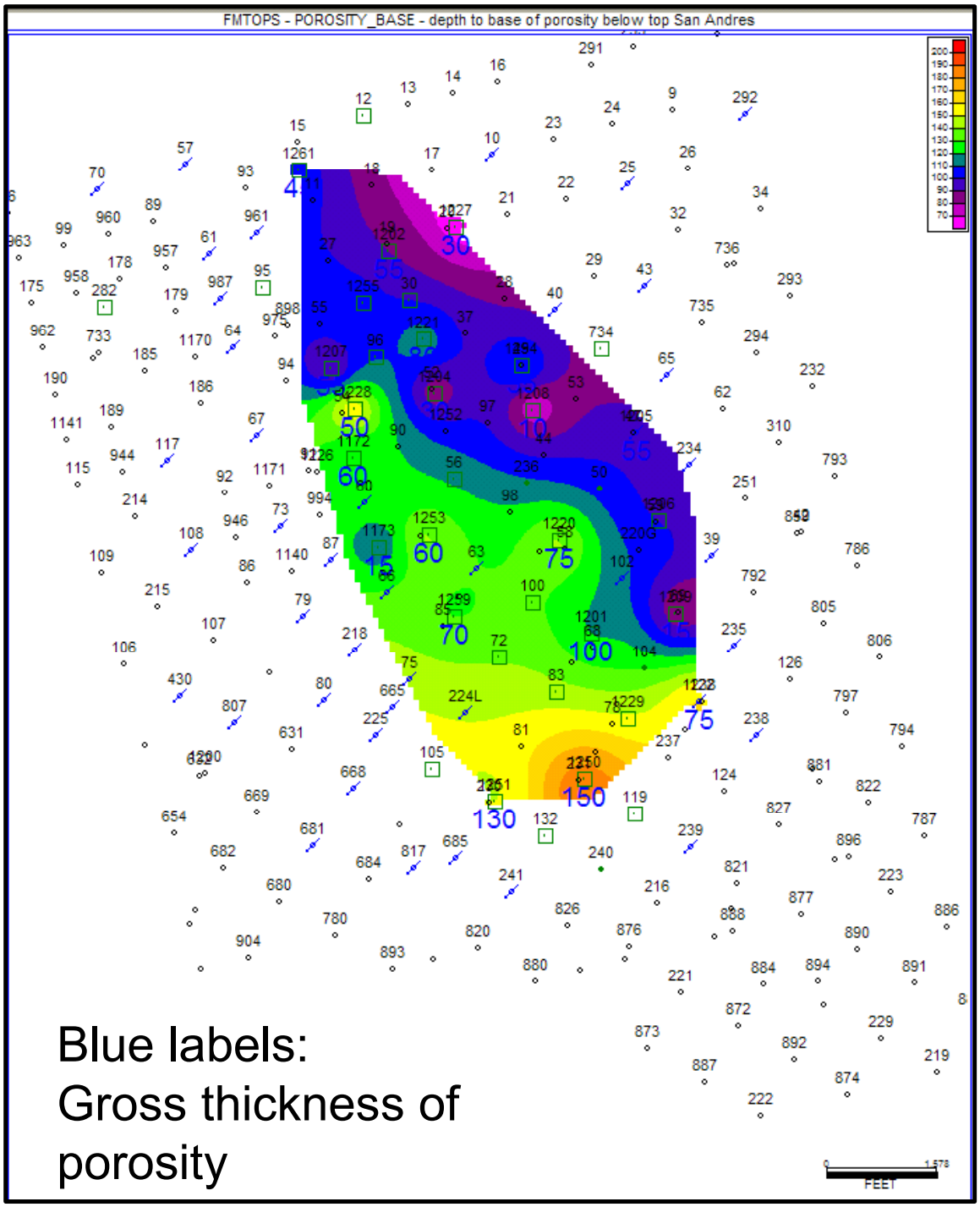

Figure 2.8. Depth from the top of San Andres Formation to the base of the porous carbonate with >10% porosity that lies above the "x" marker.

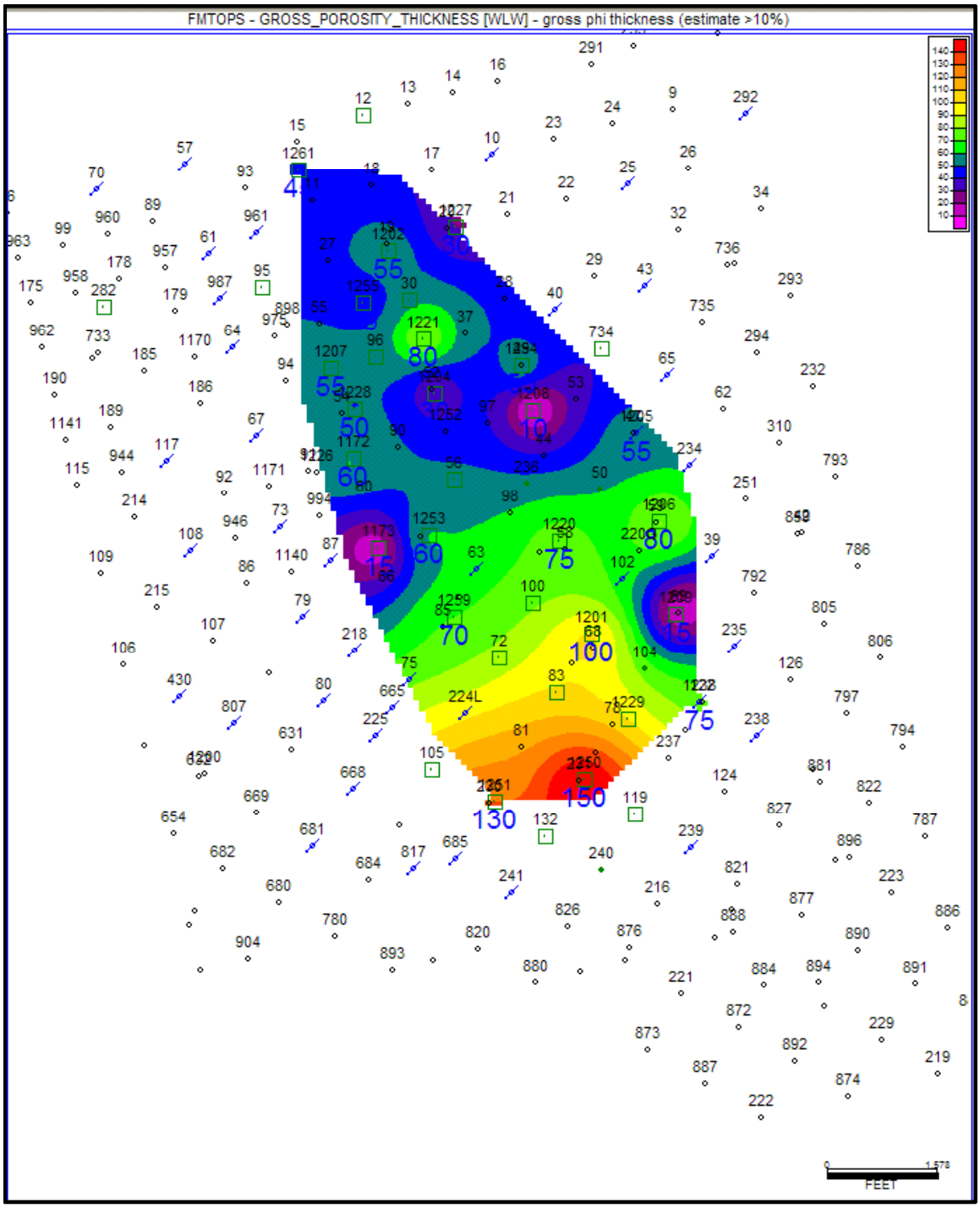

Figure 2.9. Gross thickness of the interval with >10% porosity.

C C’

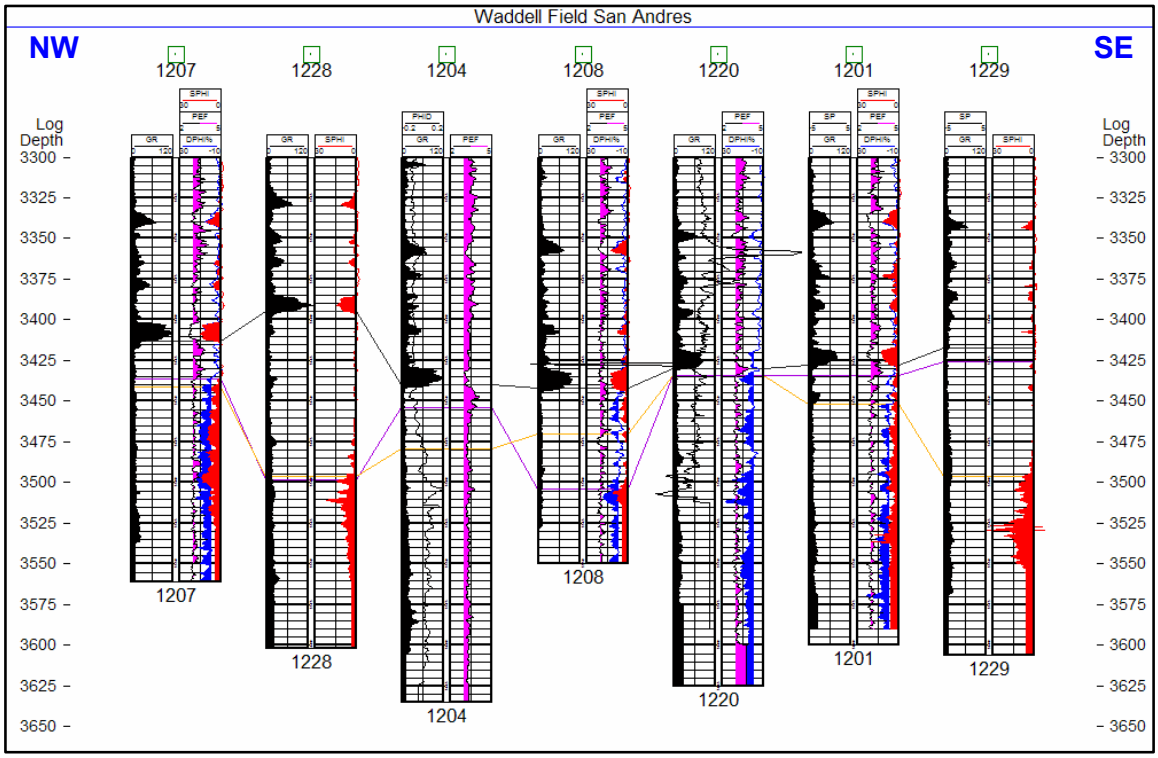

Figure 2.10. NW-SE structural cross section C-C’. Index map is provided in Figure 2.1. The base of the “tight” zone beneath the top of San Andres is defined by an orange-colored line. The base of the anhydritic section is defined by the purple-colored line. The top of the San Andres Formation is identified with a black line. Note that depths of the tight zone and anhydritic section do vary considerably relative to the top of the San Andres Formation. The tight and anhydritic zones were computed from well logs using a statistical zonation program..

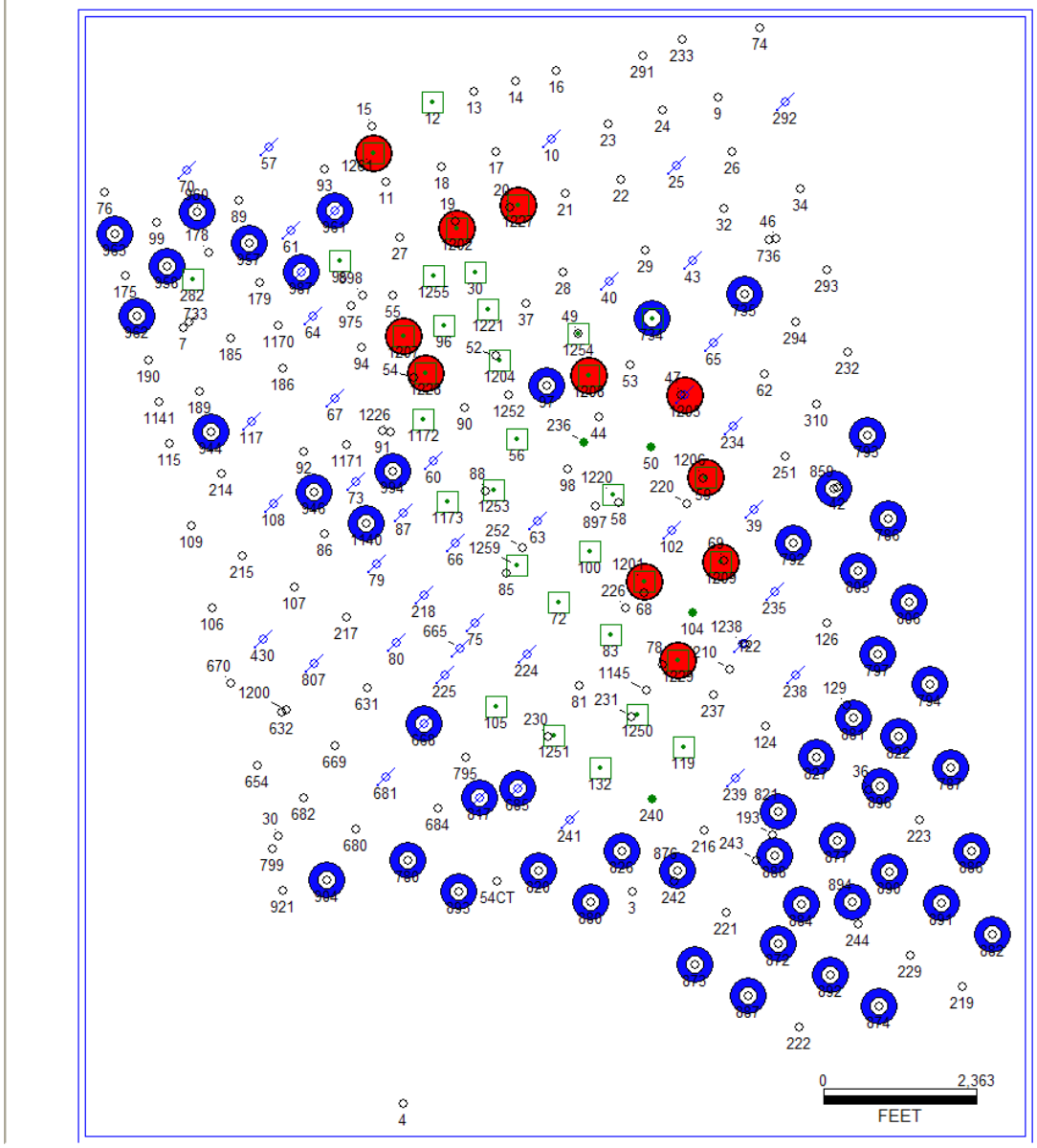

Figure 2.11. Locations of wells in the Waddell Field study area with sonic logs (blue) and both sonic and density logs (red).

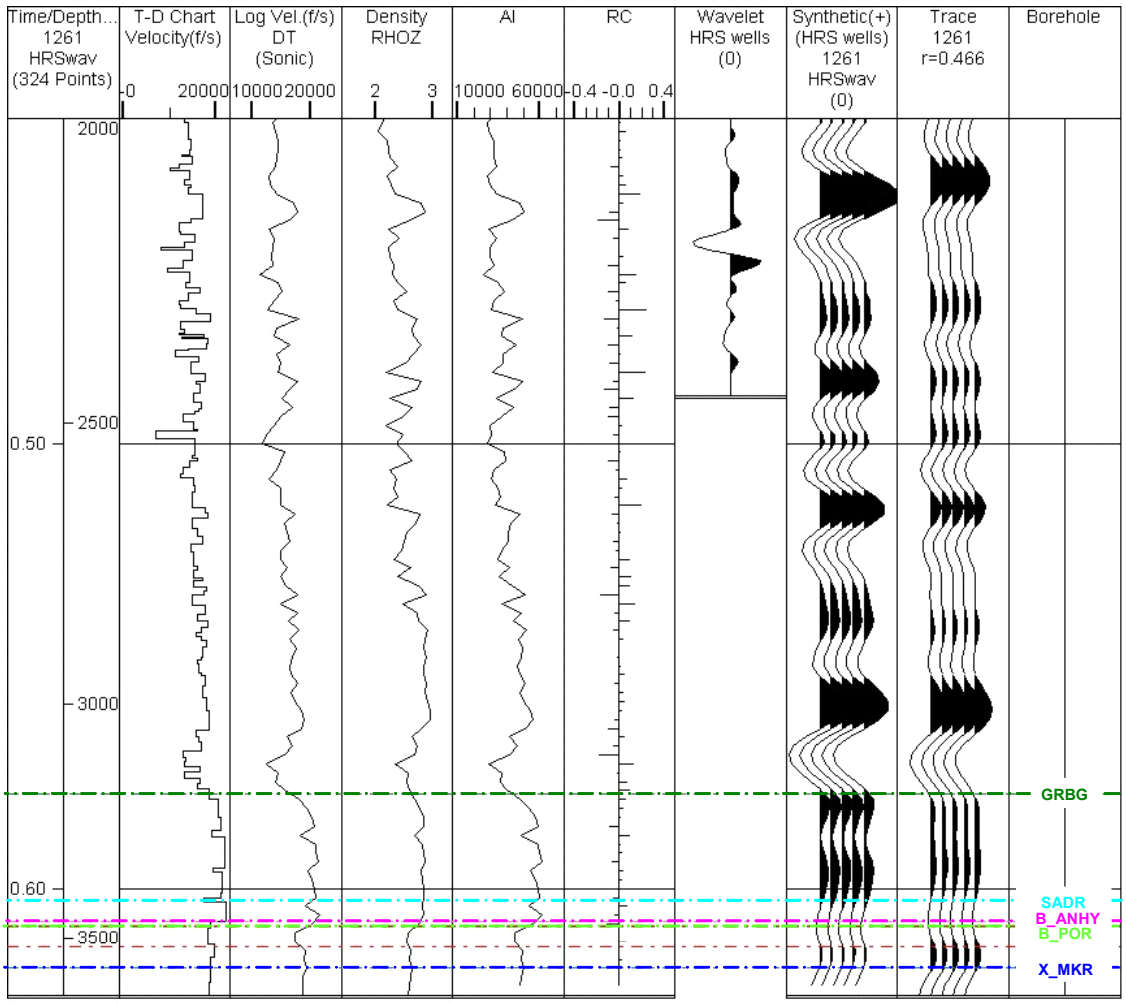

Figure 2.12. Synthetic seismogram for Waddell #1261 showing tie with seismic data. Labeled tops are: top Grayburg (GRBG; dark green), top San Andres (SADR; cyan), base of anhydritic section beneath the top of San Andres (B_ANHY; magenta), base of tight zone beneath top of San Andres (B_POR; light green), "x" marker (X_MKR; blue).

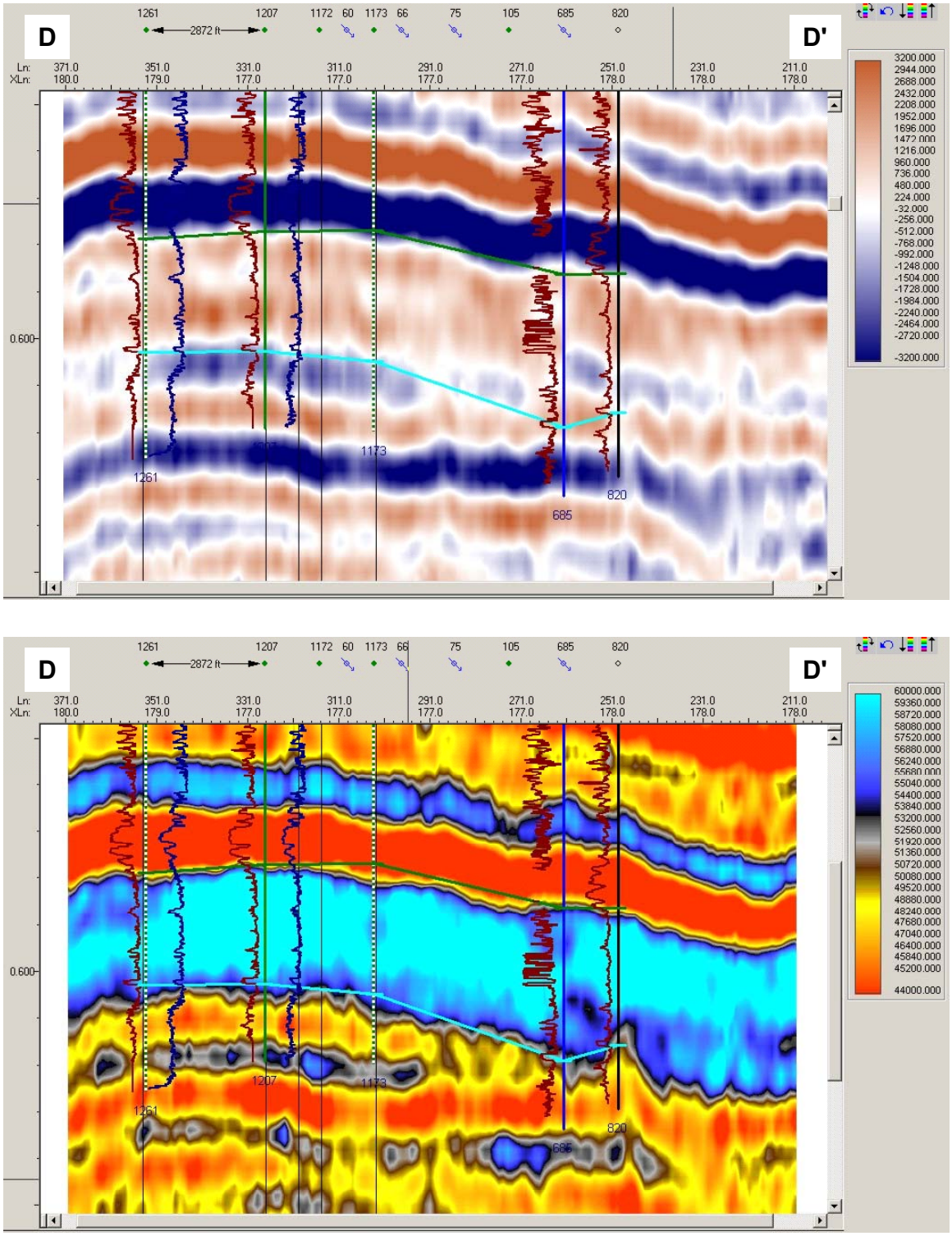

Figure 2.13. Vertical section D-D' (located in Figure 2.14) through the East Ranch seismic amplitude volume (top) and an acoustic impedance volume (bottom) generated from the East Ranch seismic data using model based inversion. The top Grayburg (green) and top San Andres (cyan) formation tops are shown connected by straight lines. Well logs displayed are sonic (dark red) and density (dark blue).

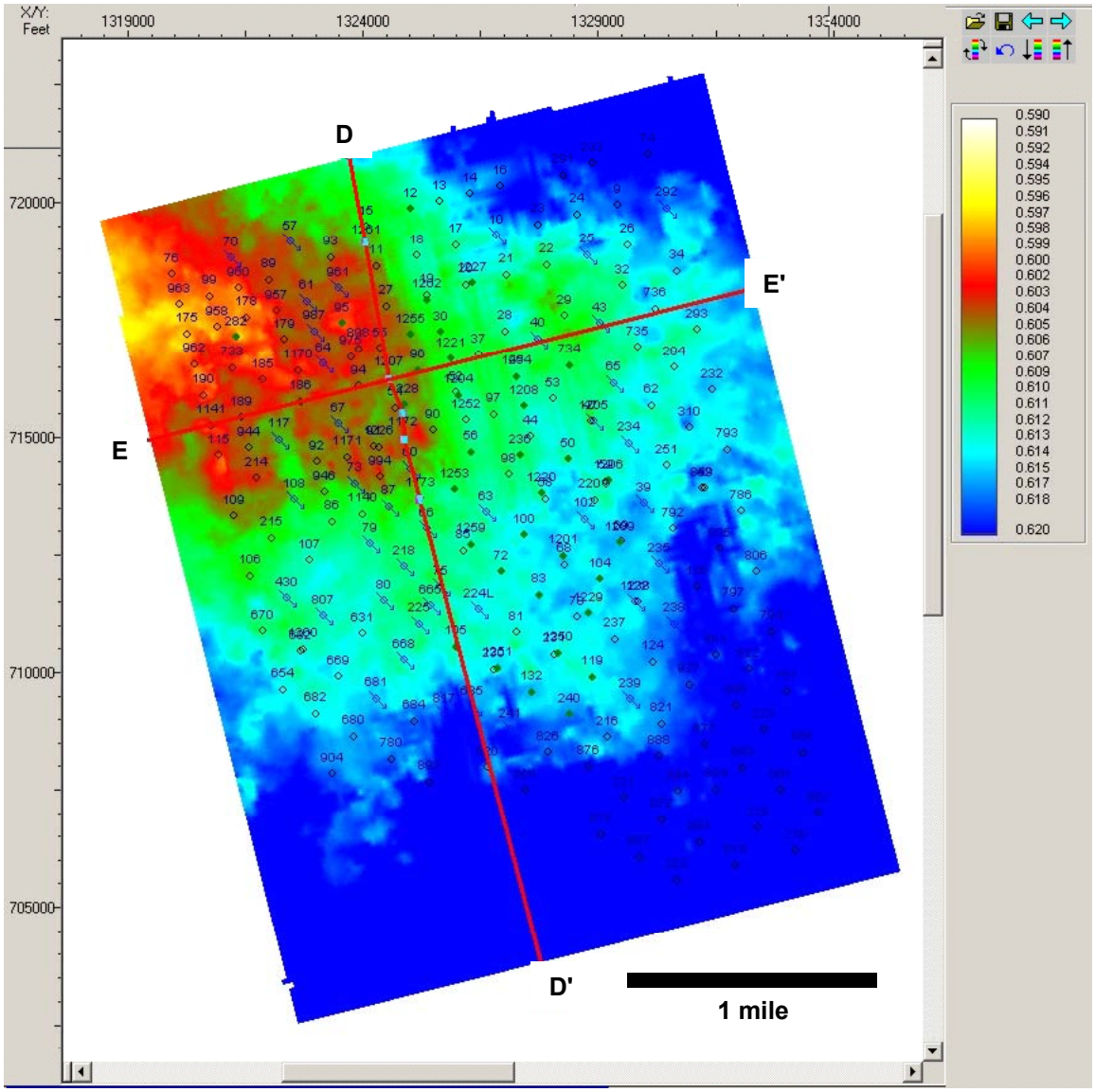

Figure 2.14. Time structure map of the "San Andres" horizon, which is believed to correspond to the base of the anhydritic karst interval at the top of the San Andres Formation. Cross sections D-D' (shown in Figures 2.13 and 2.16) and E-E' (shown in Figure 2.16) are located.

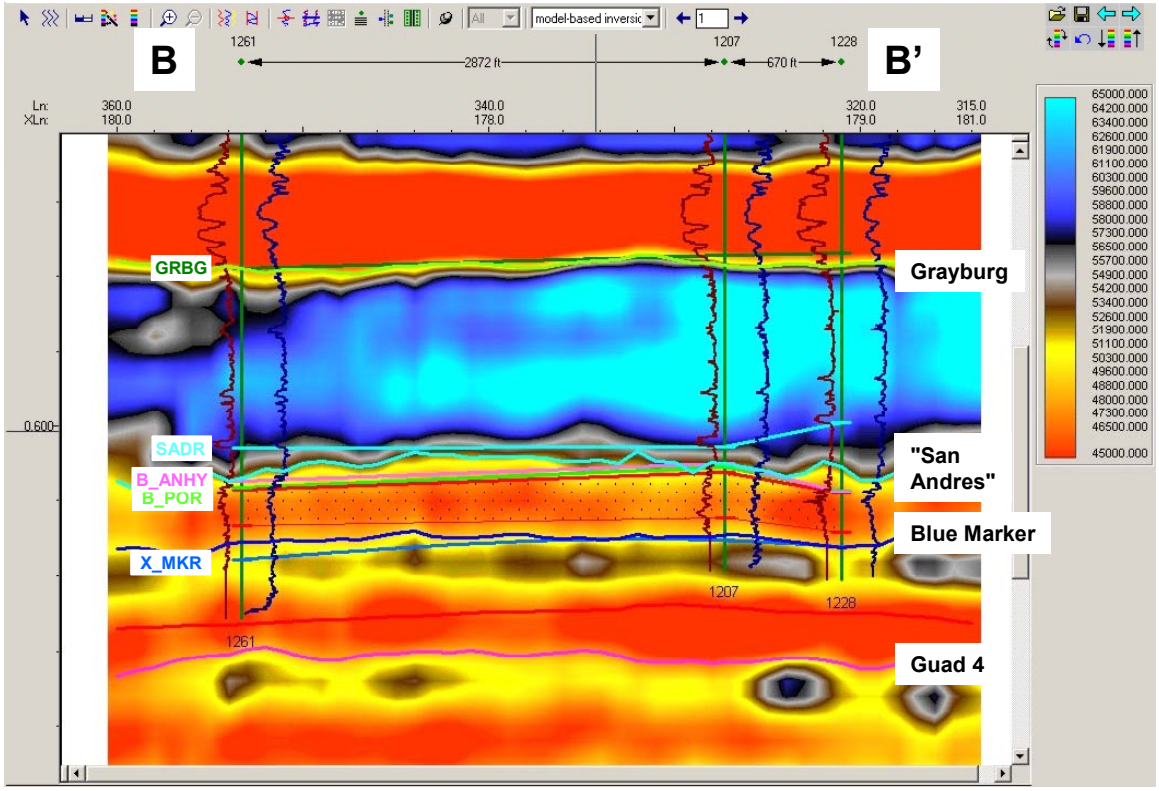

Figure 2.15. Vertical section B-B', corresponding to the well cross section shown in Figure 2.3 and located in Figure 2.1, through the East Ranch acoustic impedance volume. Synthetic seismograms from sonic (dark red) and density (dark blue) logs were used to tie well depths to seismic times and correlate formation tops with seismic horizons. Displayed well tops, connected by straight lines, are as in Figure 2.12. The dotted fill corresponds to the porous interval with >10% porosity. Horizons interpreted from the impedance volume are Grayburg (light green), "San Andres" (cyan), blue marker (blue), and Guad 4 (magenta). Note that the "San Andres" horizon corresponds more closely to the base of the anhydrite (or base of the tight zone) than to the top of the San Andres Formation.

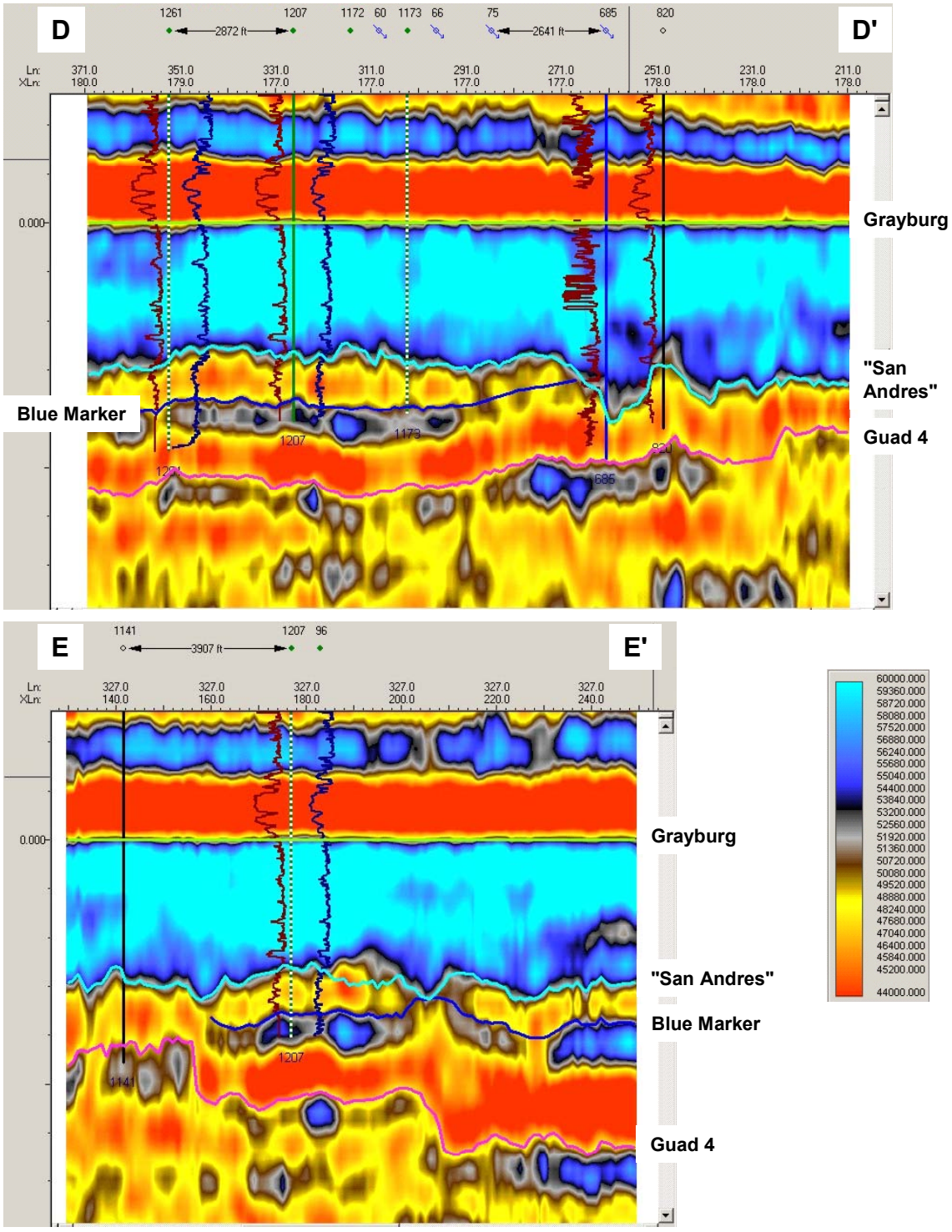

Figure 2.16. Vertical sections D-D' (top) and E-E' (bottom), flattened on the Grayburg horizon, through the East Ranch acoustic impedance volume. Note that the "blue" marker horizon, which appears to correspond to the "x" marker identified from logs, is truncated by the "San Andres" base of karst horizon at several locations. Sections are located in Figure 2.14.

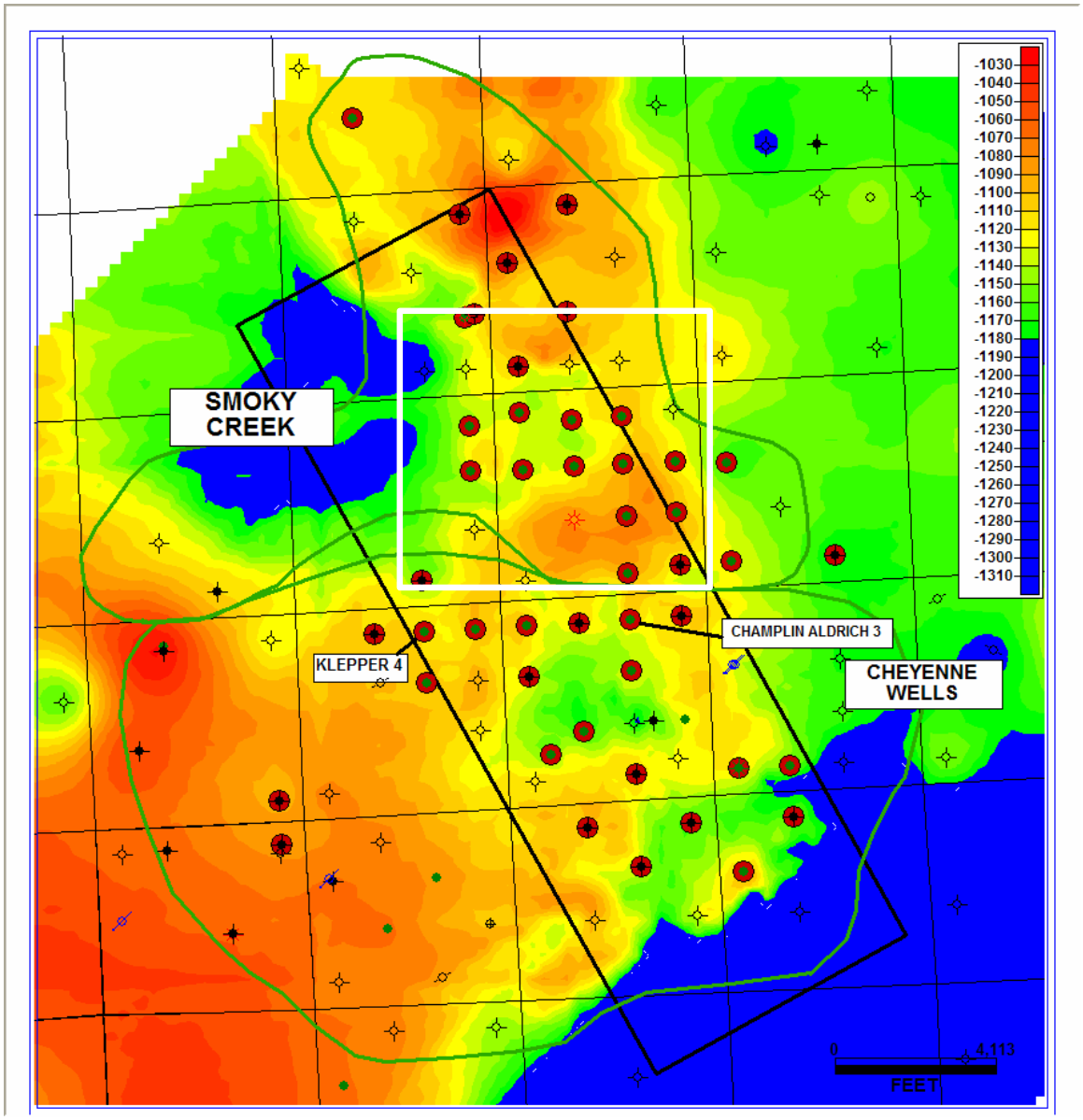

Figure 3.1. Structure map of the top of Spergen in the Mississippian study area, enhanced by seismic control within the 3D seismic outline (heavy black rectangle) using the original processed data. The outlines of the Smoky Creek and Cheyenne Wells fields are shown in green. Wells with Spergen production are highlighted in red. Cored wells are labeled. The white box shows the location of the curvature extractions in Figures 3.4, 3.5, and 3.7.

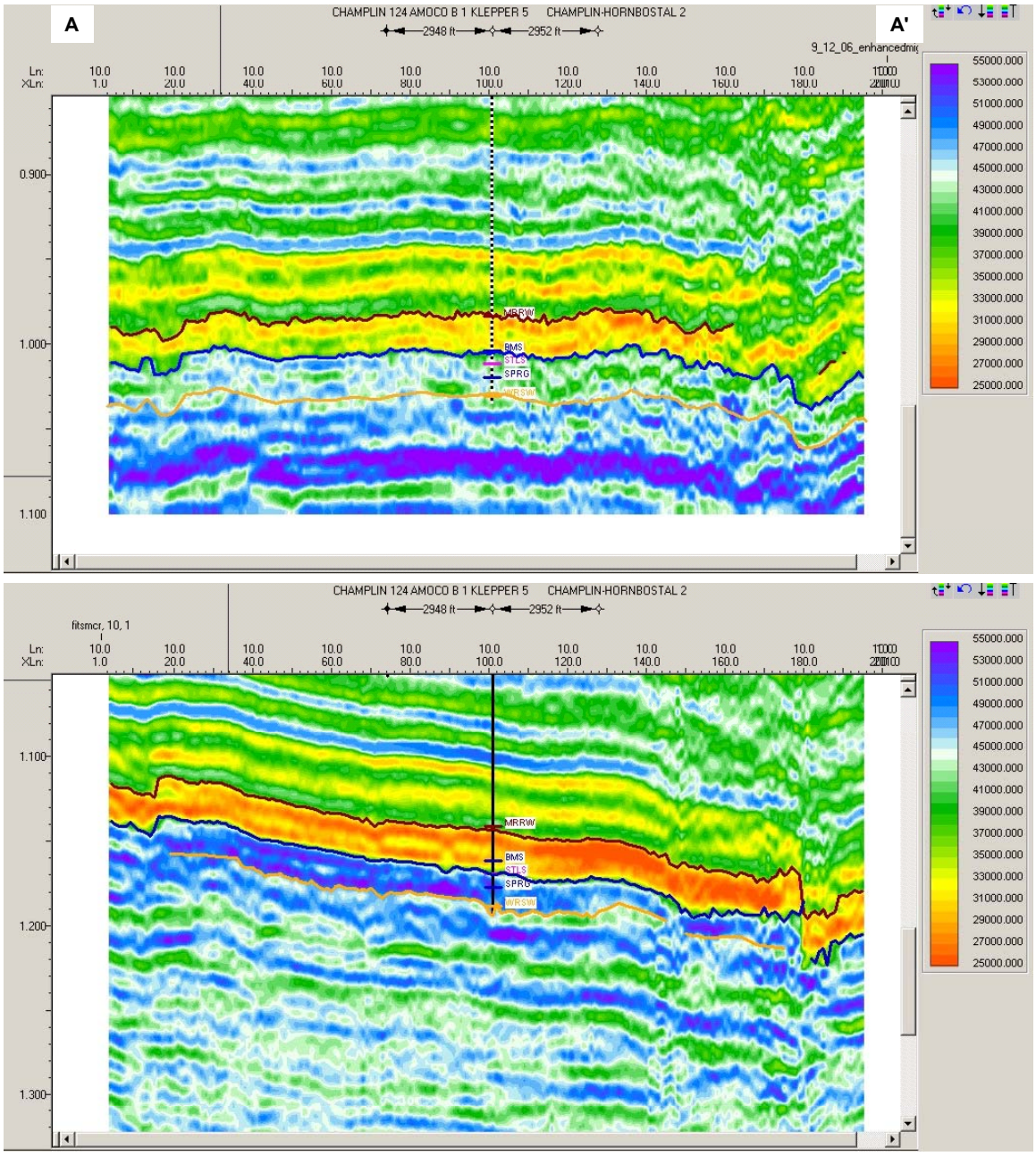

Figure 3.2. Vertical section A-A' through acoustic impedance volumes generated from model-based inversion of the original seismic data (top) and reprocessed seismic data (bottom) from the Mississippian study area. Formation tops displayed are the top Morrow (MRRW, dark red), base of Morrow shale (BMS, blue), top St. Louis (STLS, magenta), top Spergen (SPRG, dark blue), and top Warsaw (WRSW, gold). Interpreted seismic horizons are the Morrow (dark red), BMS (blue), and Warsaw (gold).

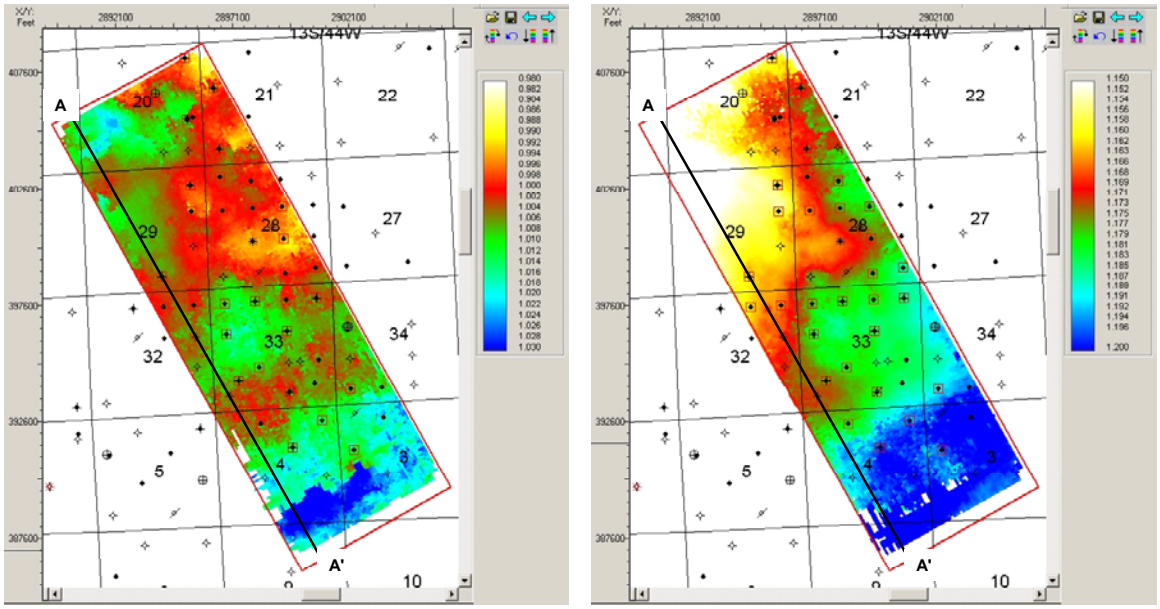

Figure 3.3. Time structure map of the BMS horizon, interpreted from the original seismic data (left) and the reprocessed seismic data (right) in the Mississippian study area. The location of seismic section A-A' (shown in Figure 3.2) is indicated by the black line.

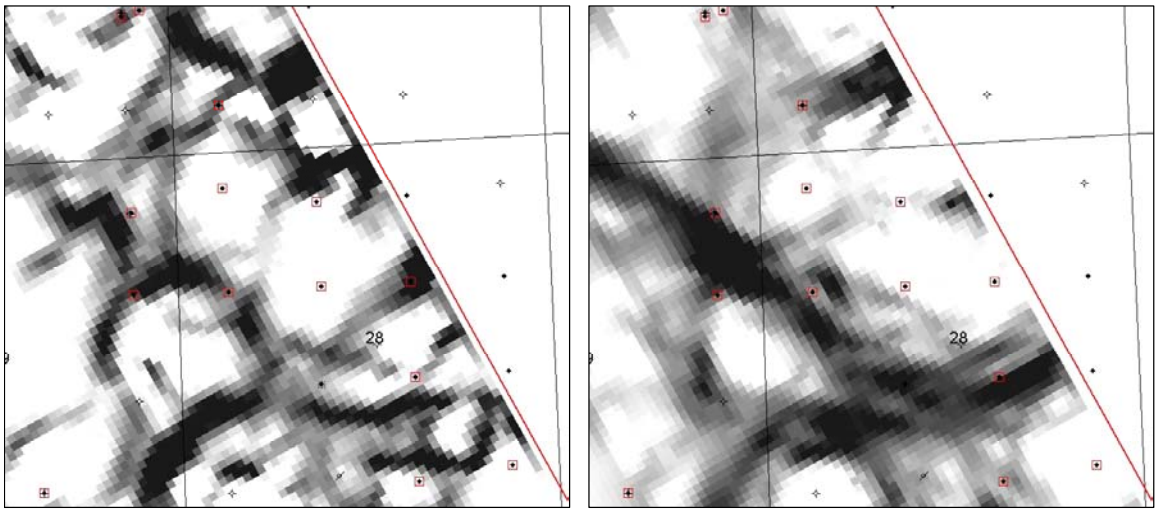

Figure 3.4. Most positive curvature for the original seismic data (left) and the re-processed seismic data (right), extracted along the approximate level of the top of Spergen. The location of these maps is shown in Figure 3.1.

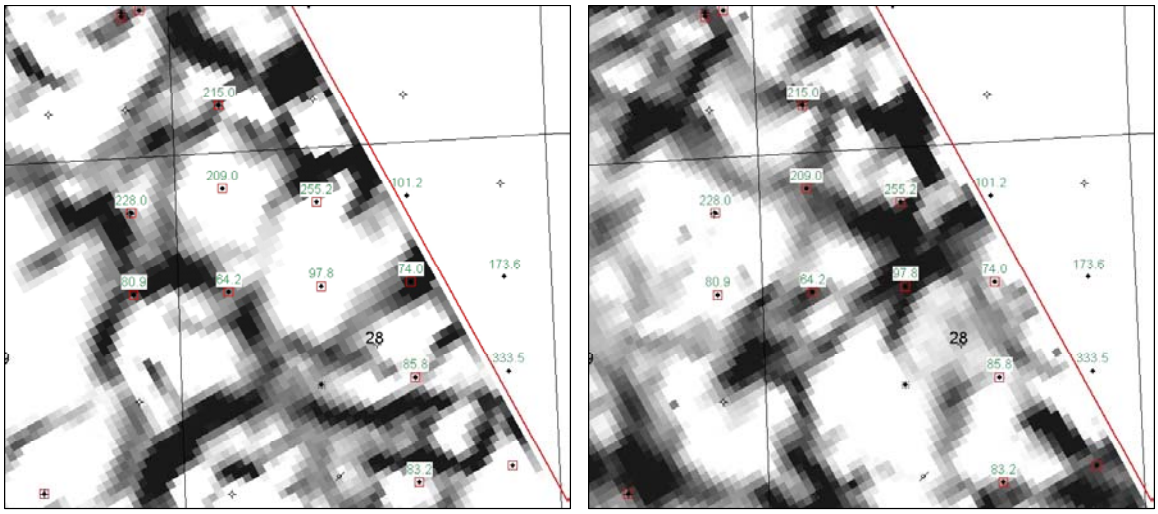

Figure 3.5. Most positive curvature (left) and most negative curvature (right) for the original seismic data, extracted along the approximate level of the top of Spergen. Cumulative oil production for Spergen producing wells is annotated in green. The location of these maps is shown in Figure 3.1.

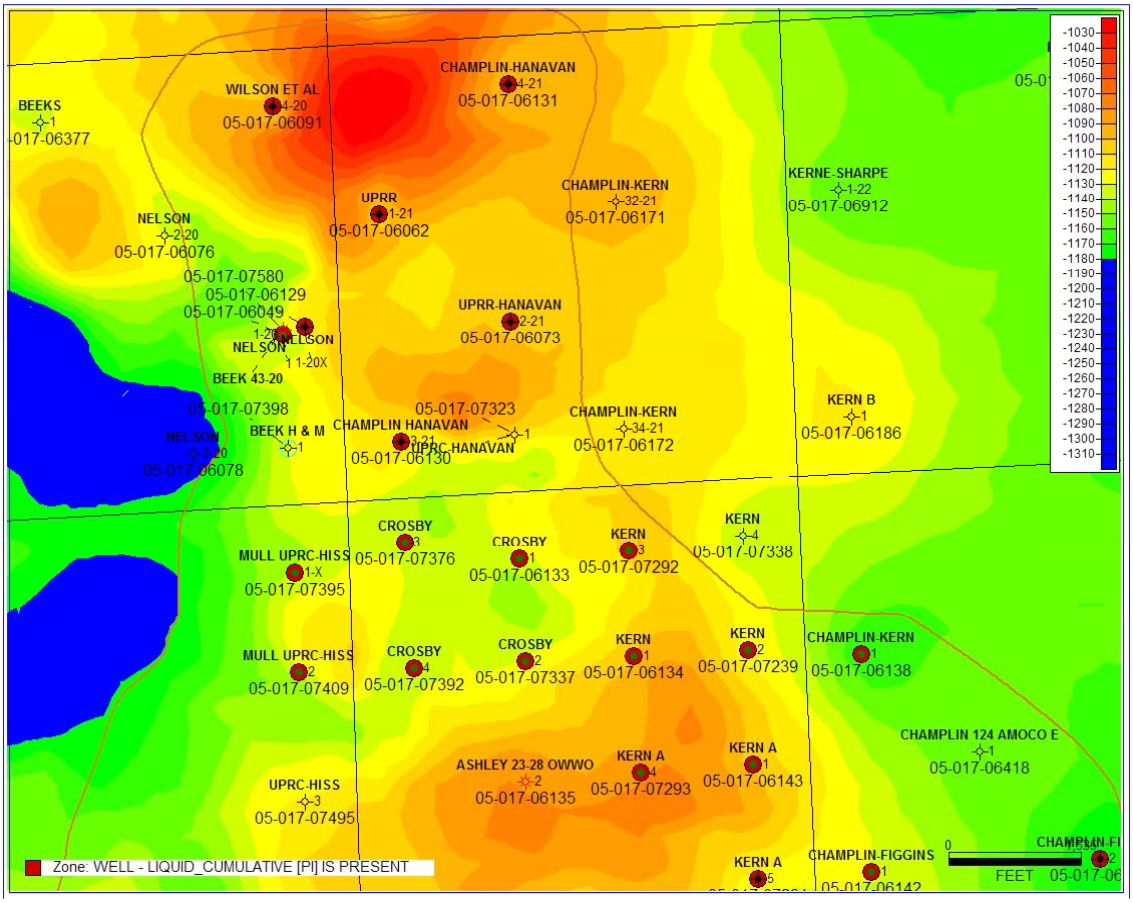

Figure 3.6. Structure map of the Spergen showing the general layout of the Smoky Creek field including well locations.

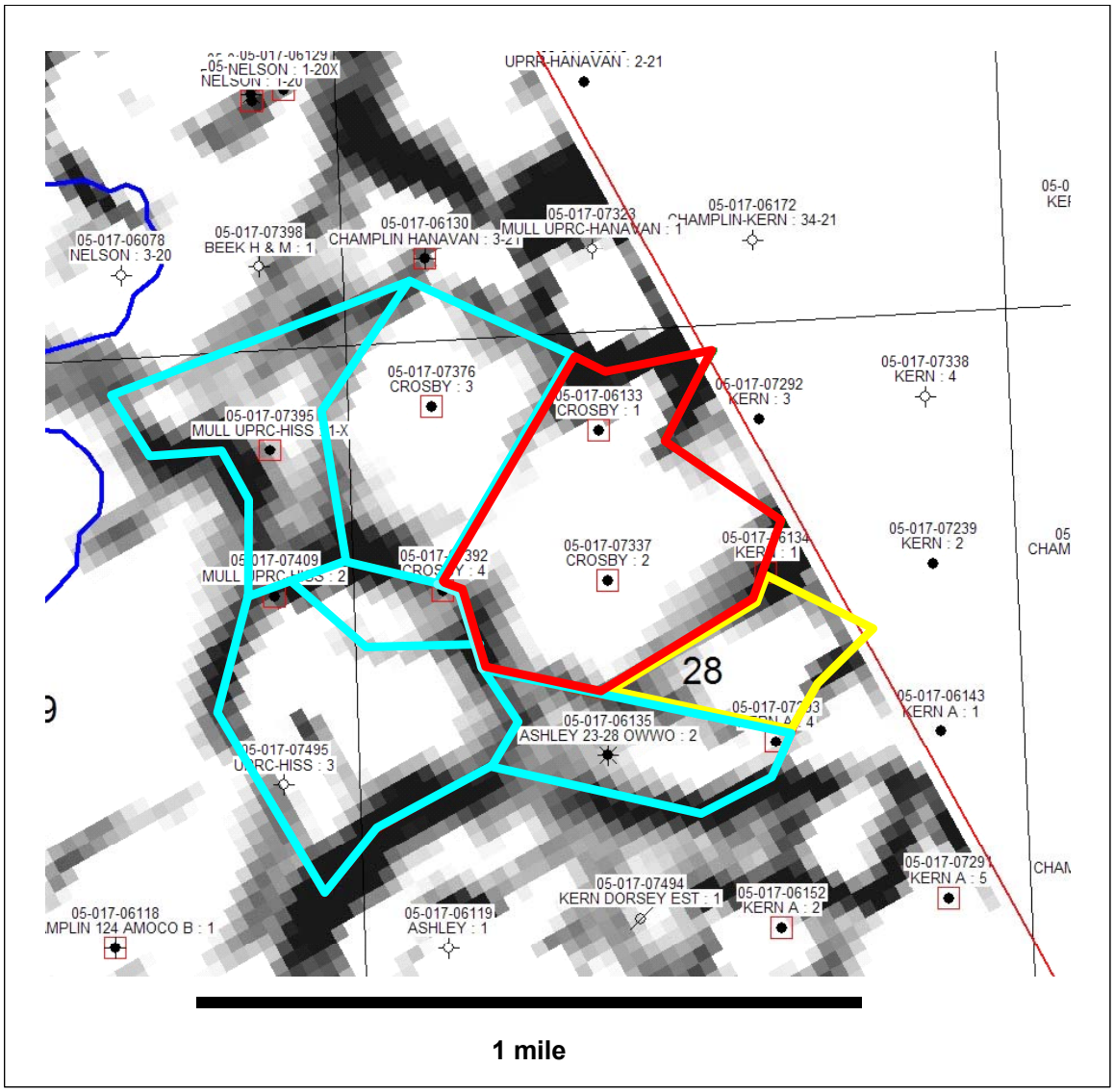

Figure 3.7. Most positive curvature map extracted along the approximate level of the top of Spergen for southern Smoky Creek field. Potential reservoir compartments within the Smoky Creek field based on this curvature map are outlined. Production for the compartment outlined in red has been simulated during the present reporting period. Based on initial success with reservoir simulation for this compartment, the five compartments outlined in blue, which each contain one Spergen producing well, will be simulated during the next reporting period. Note that the yellow compartment contains no wells and may represent untapped reservoir.

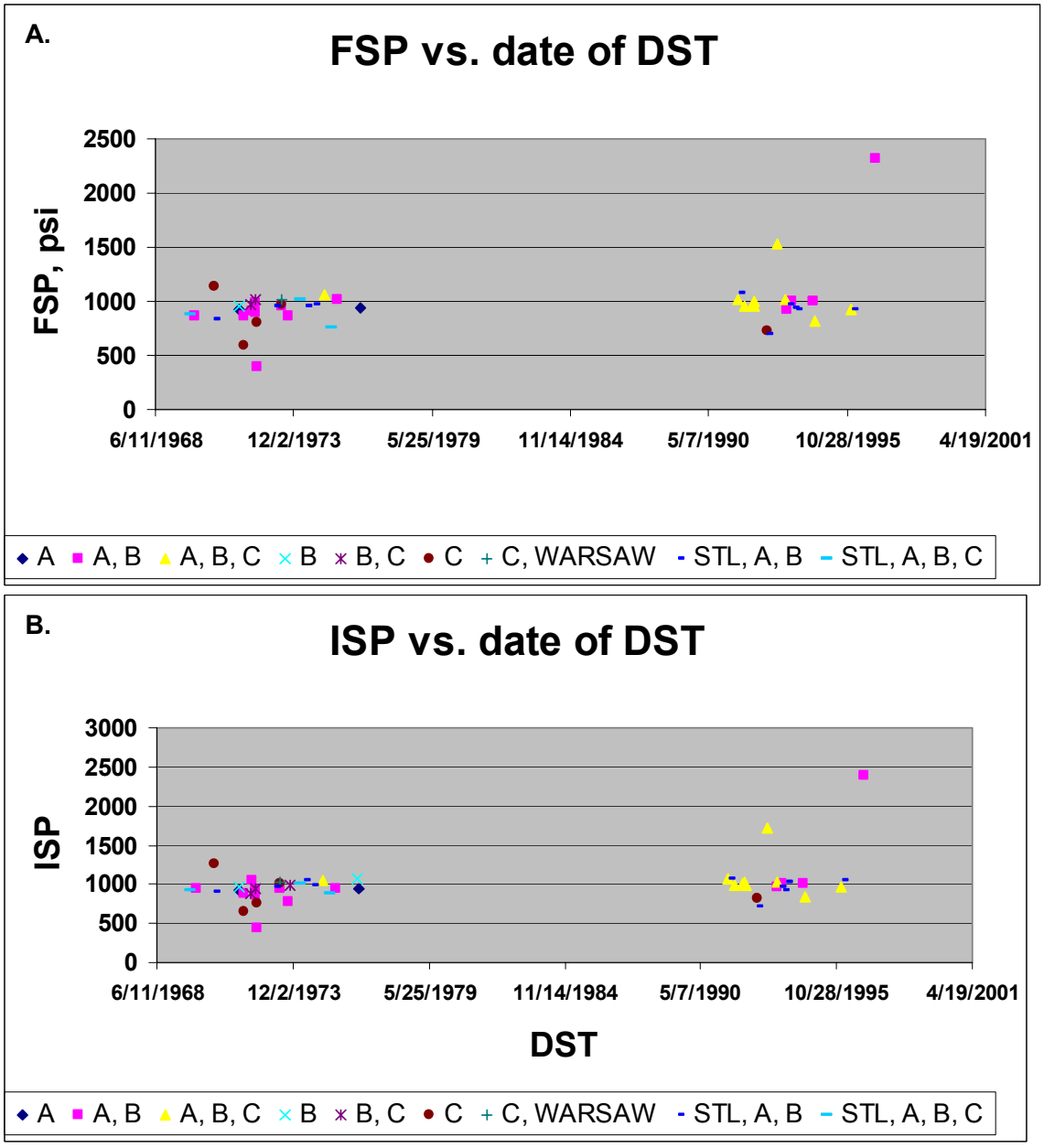

Figure 3.8. Plot of final shut-in and initial shut-in pressures from DSTs in Smoky Creek and Cheyenne Wells fields.

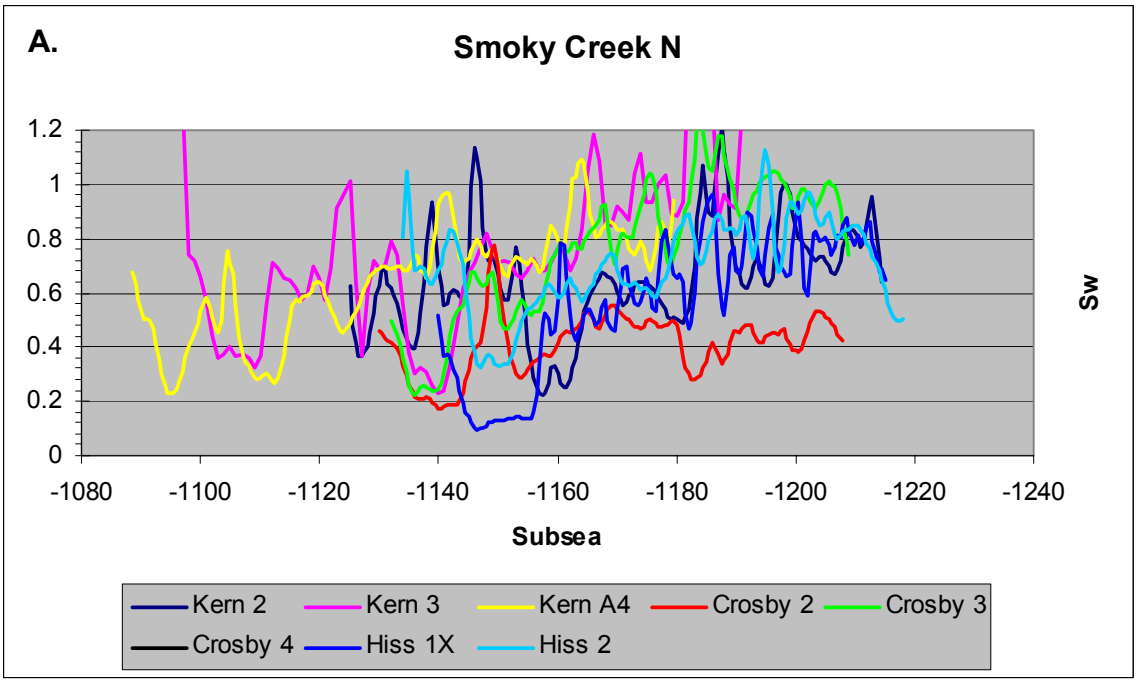

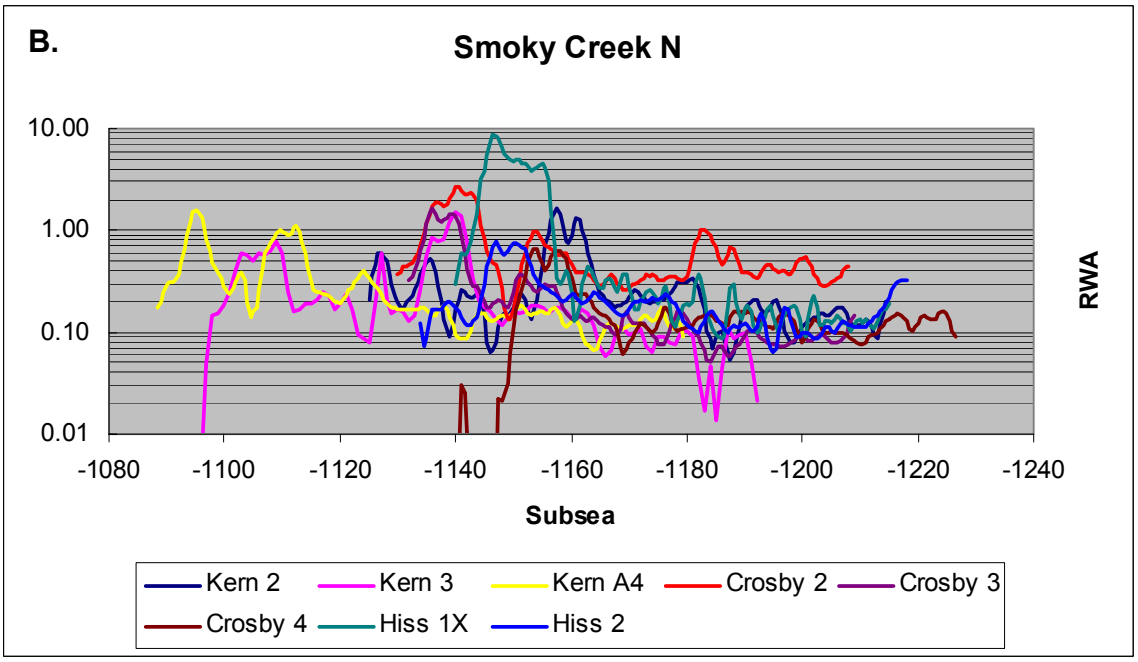

Figure 3.9. Plots of log-derived water saturation (S_w) and R_{wa} (apparent resistivity) against depth.

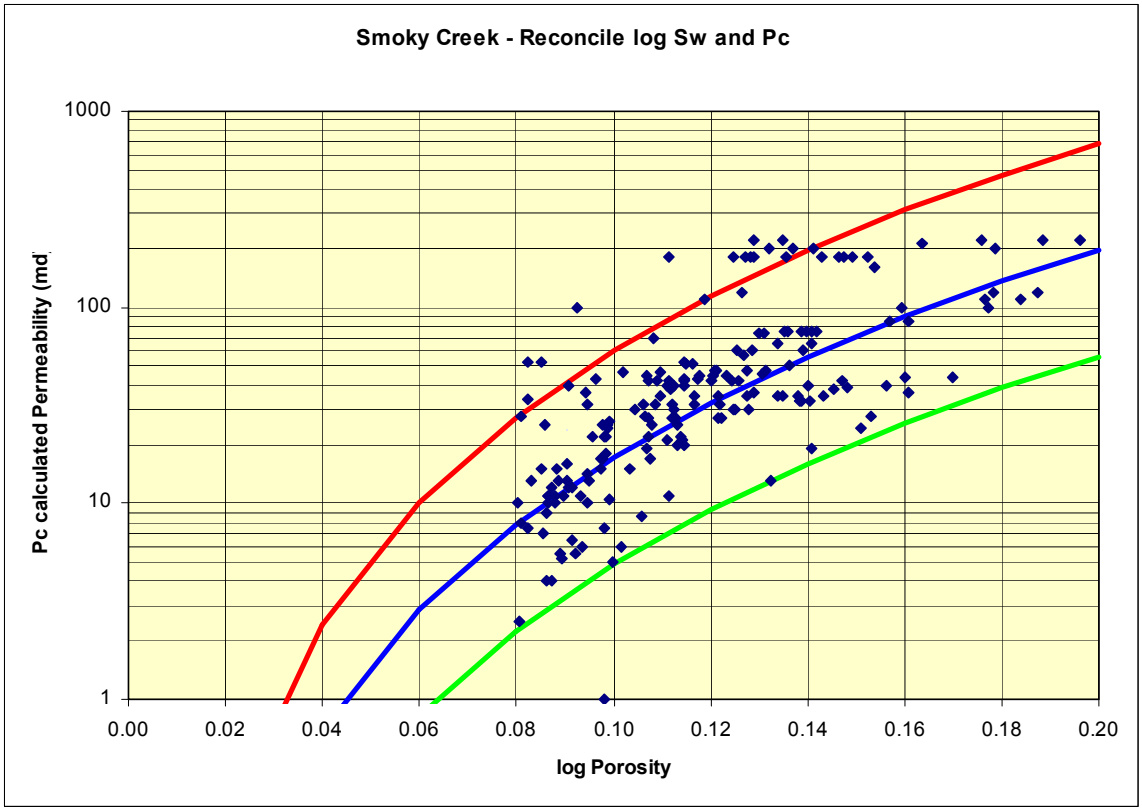

Figure 3.10. Crossplot of calculated permeability versus log-derived porosity from effective pay intervals in Smoky Creek wells.

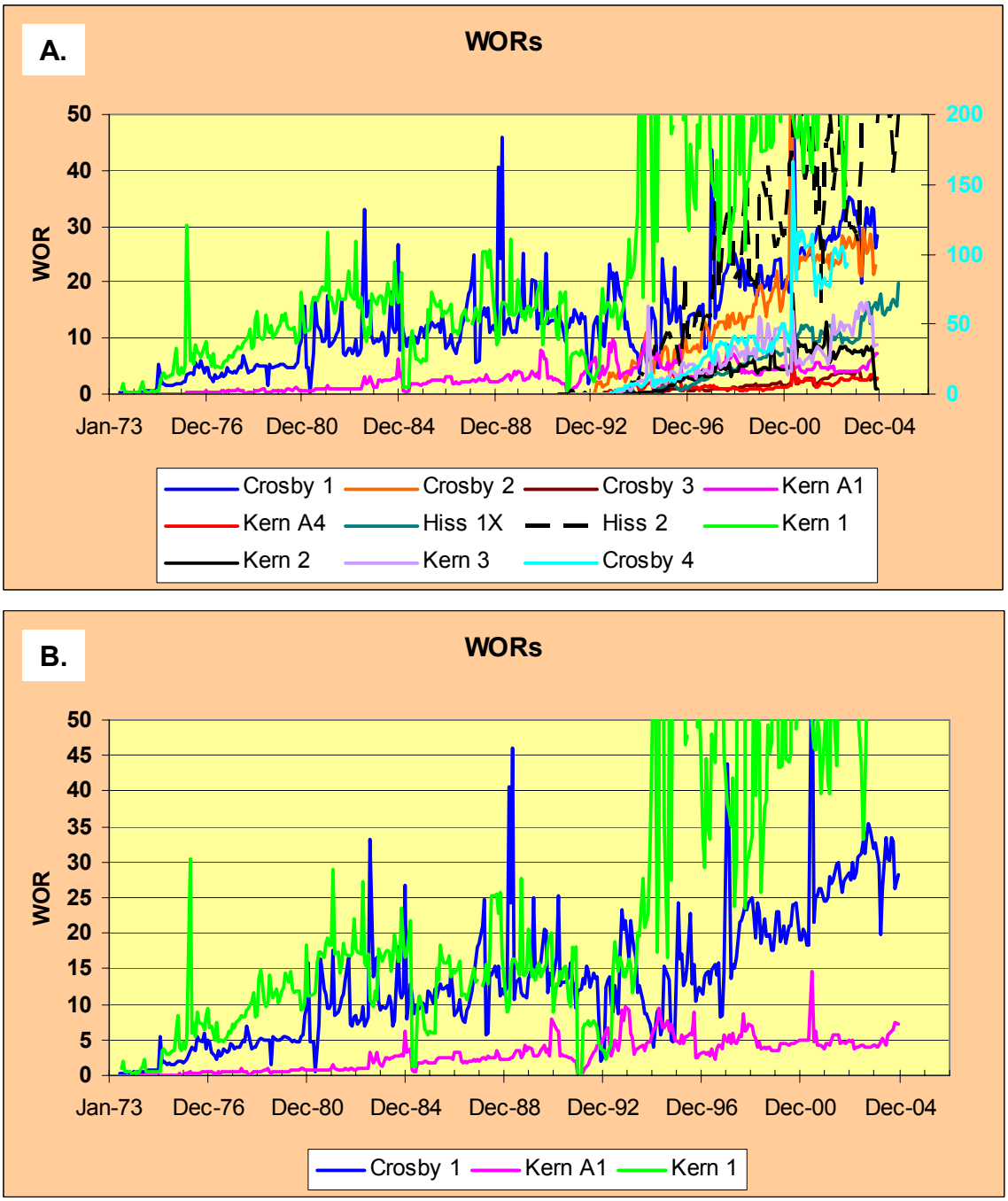

Figure 3.11. Plots of water-oil ratios against time for Smoky Creek wells.

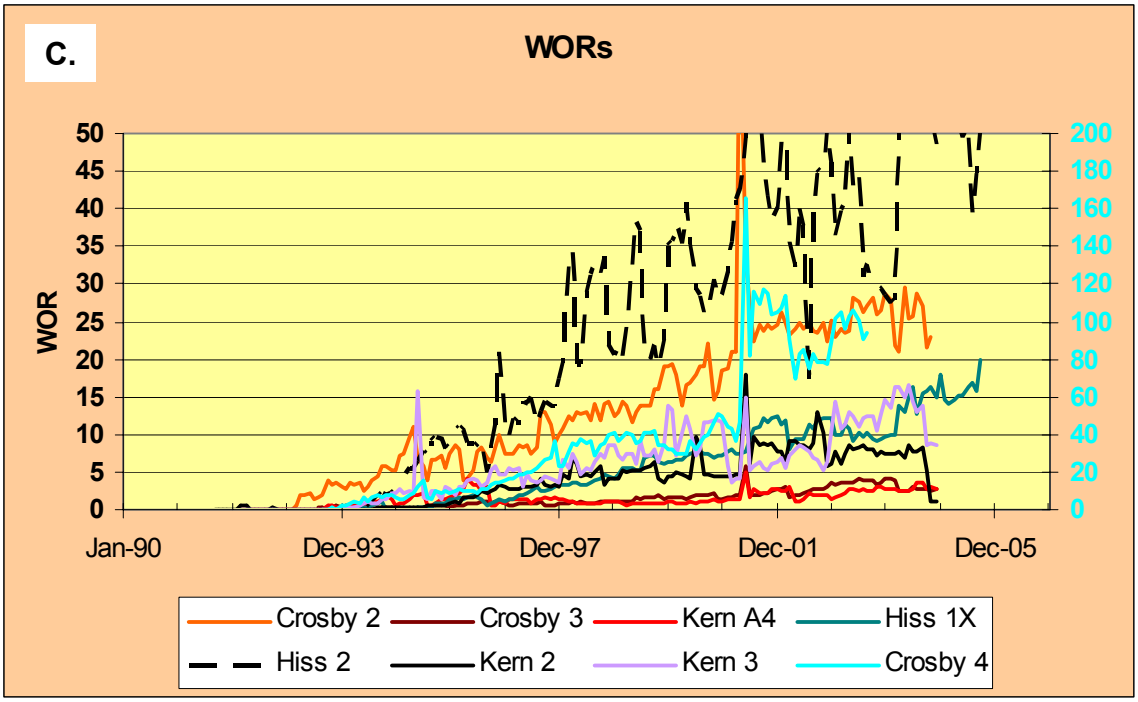

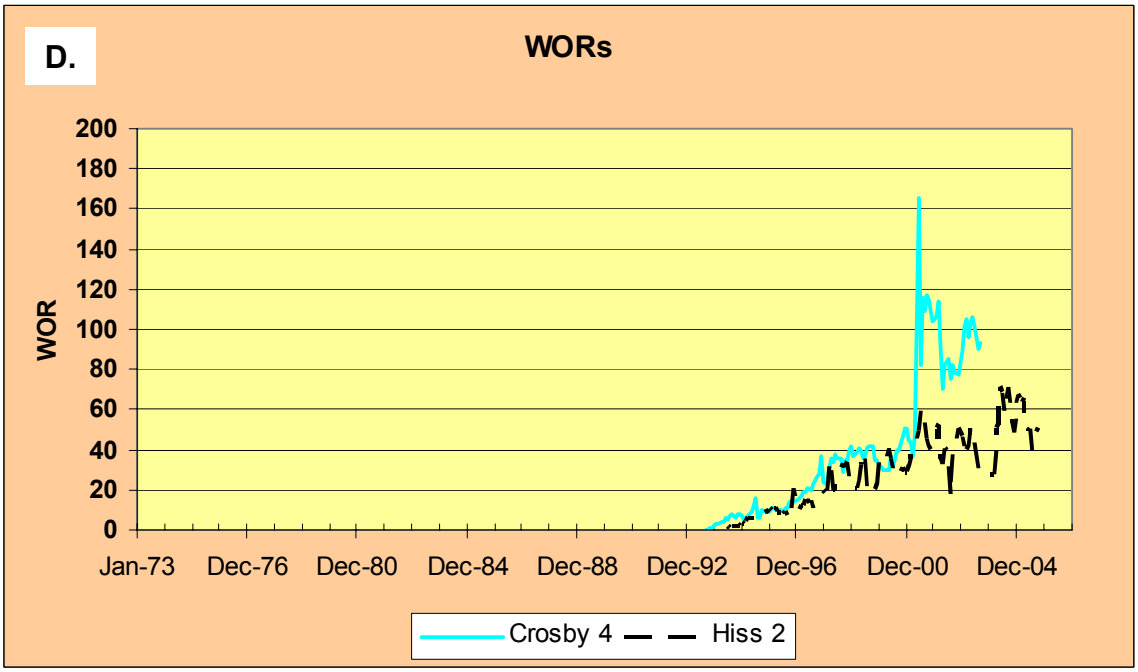

Figure 3.11. (cont.).

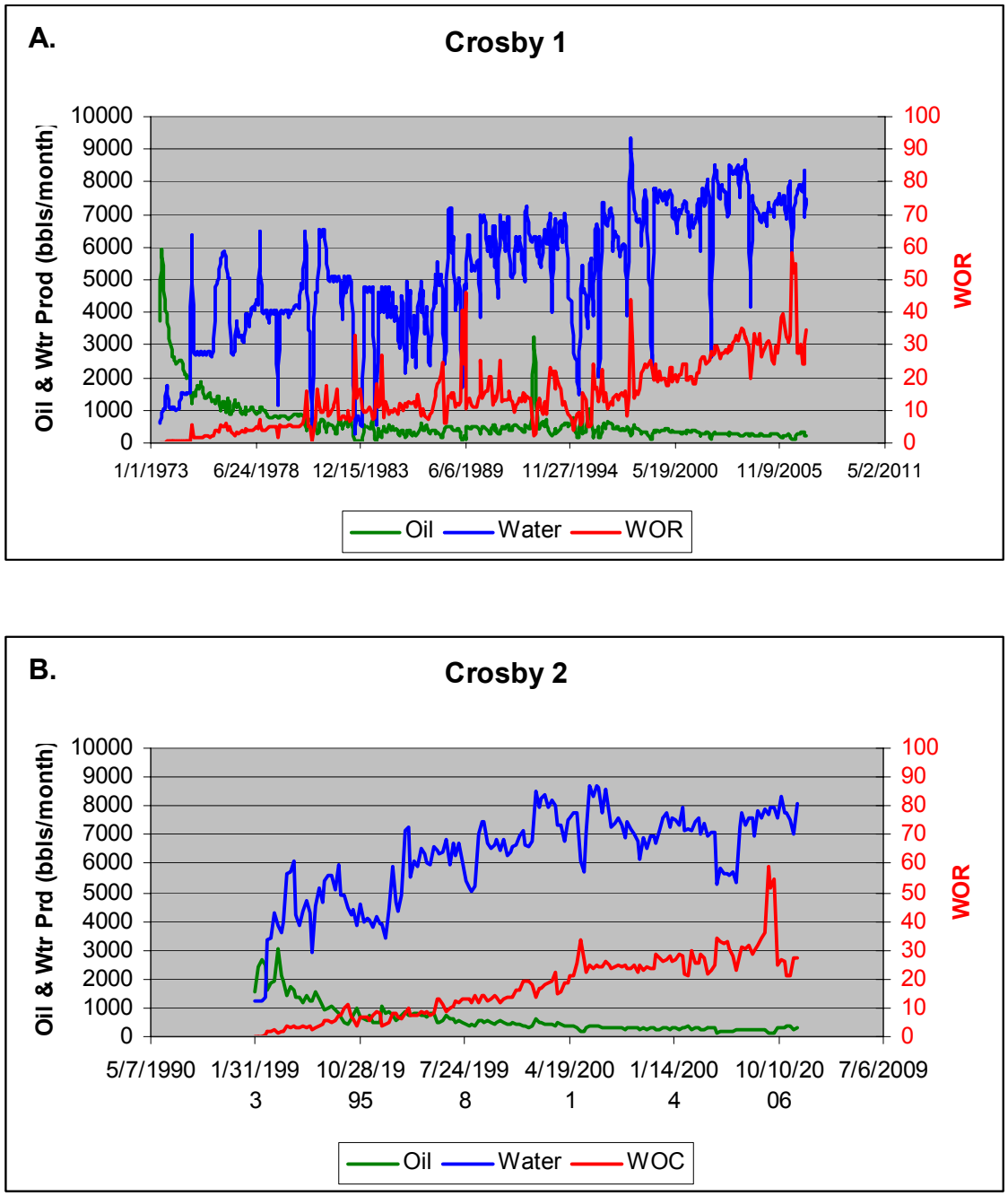

Figure 3.12. Production history of Crosby 1 and Crosby 2 wells.

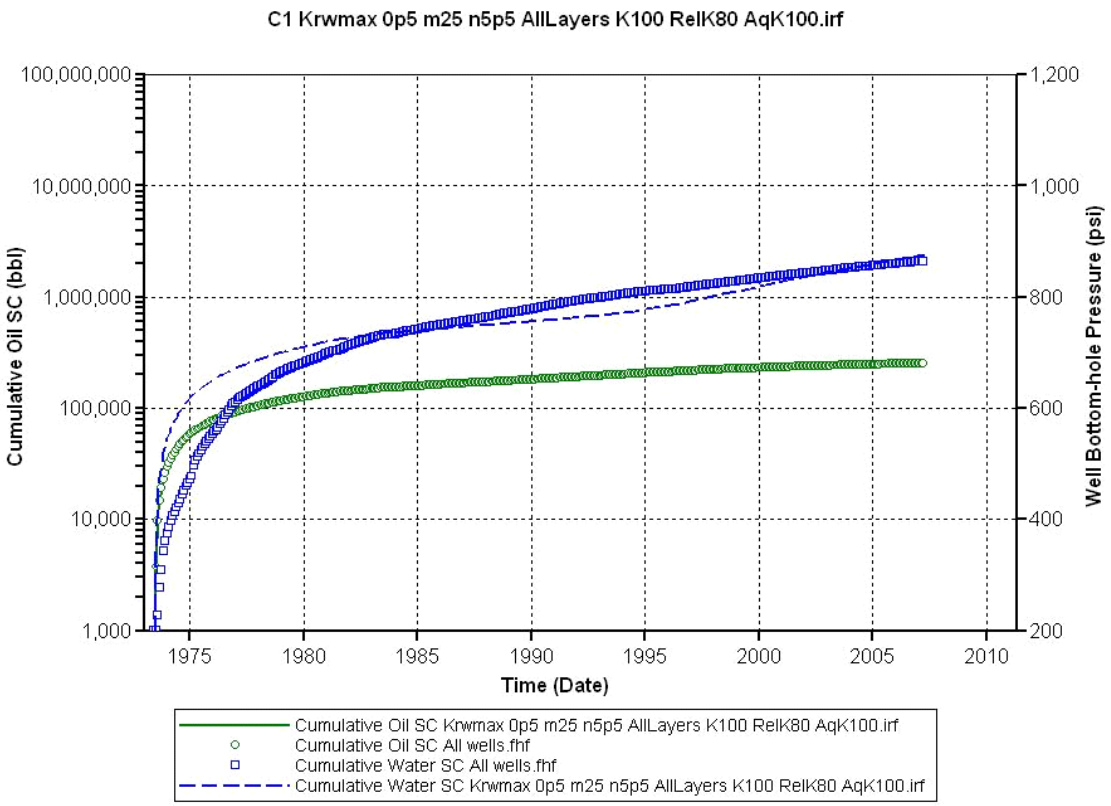

Figure 3.13. Production history-match for Crosby 1 well.

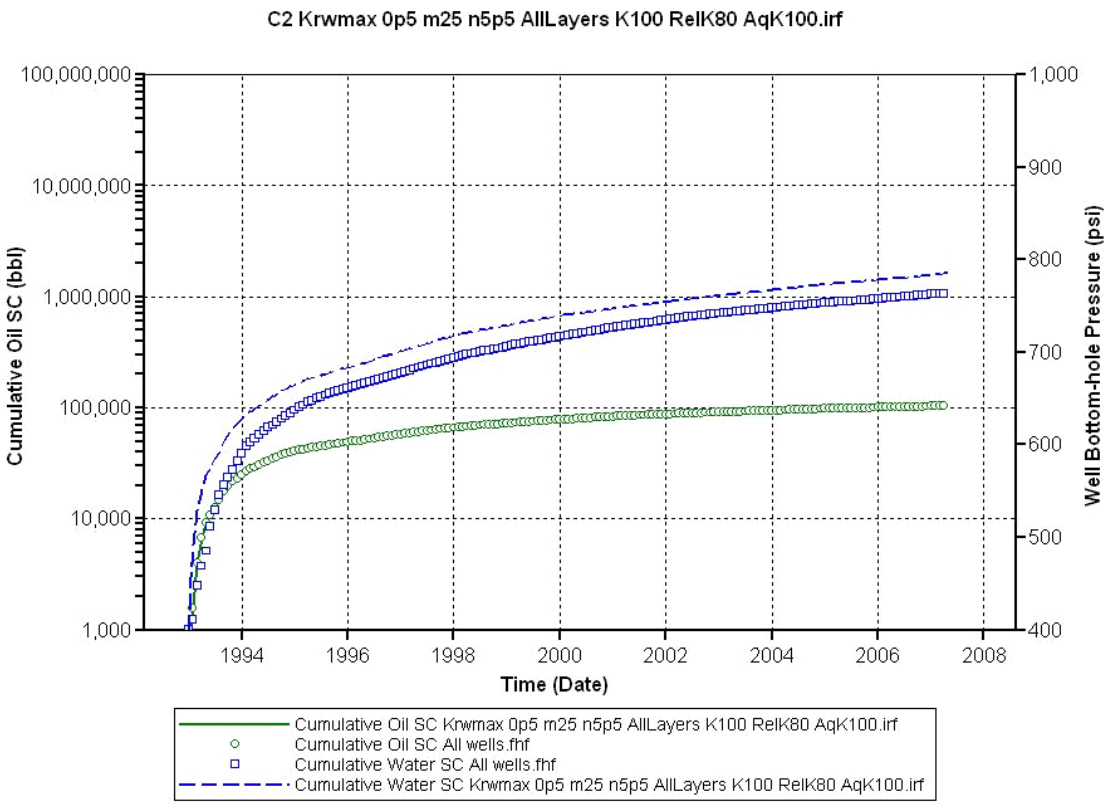

Figure 3.14. Production history-match for Crosby 2 well.

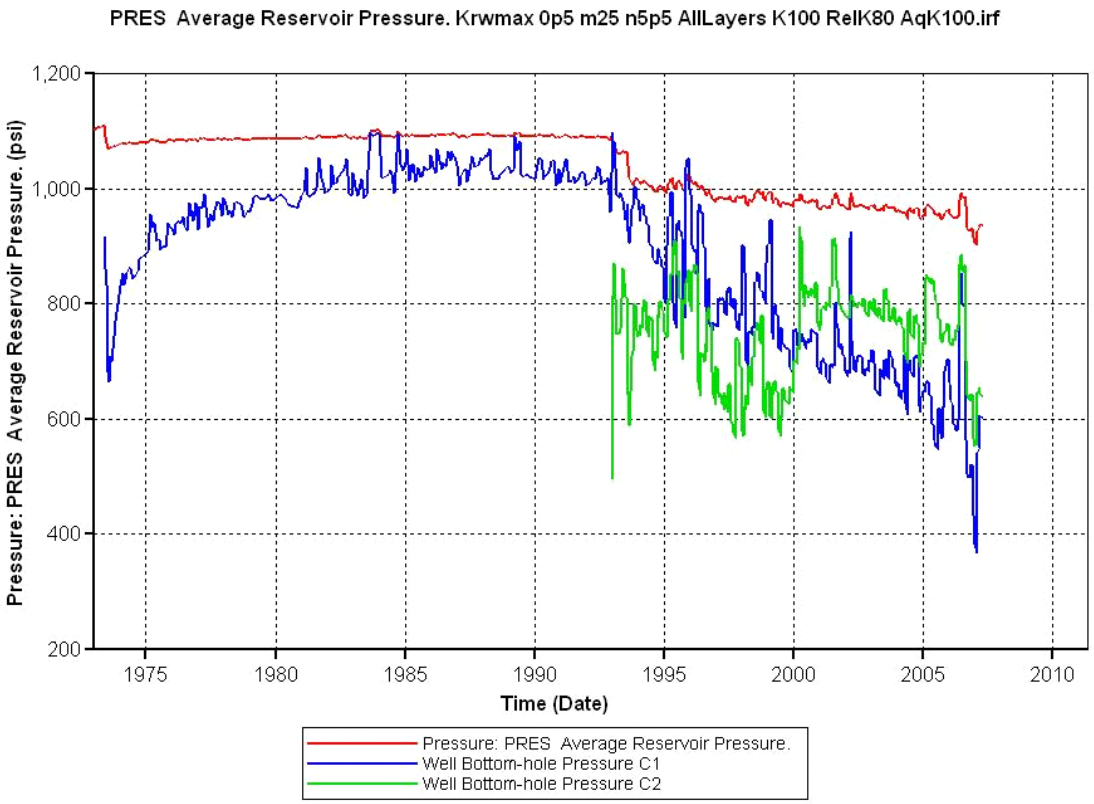

Figure 3.15. Plot of simulator-calculated average reservoir pressure and flowing bottom hole pressures in Crosby 1 and 2.

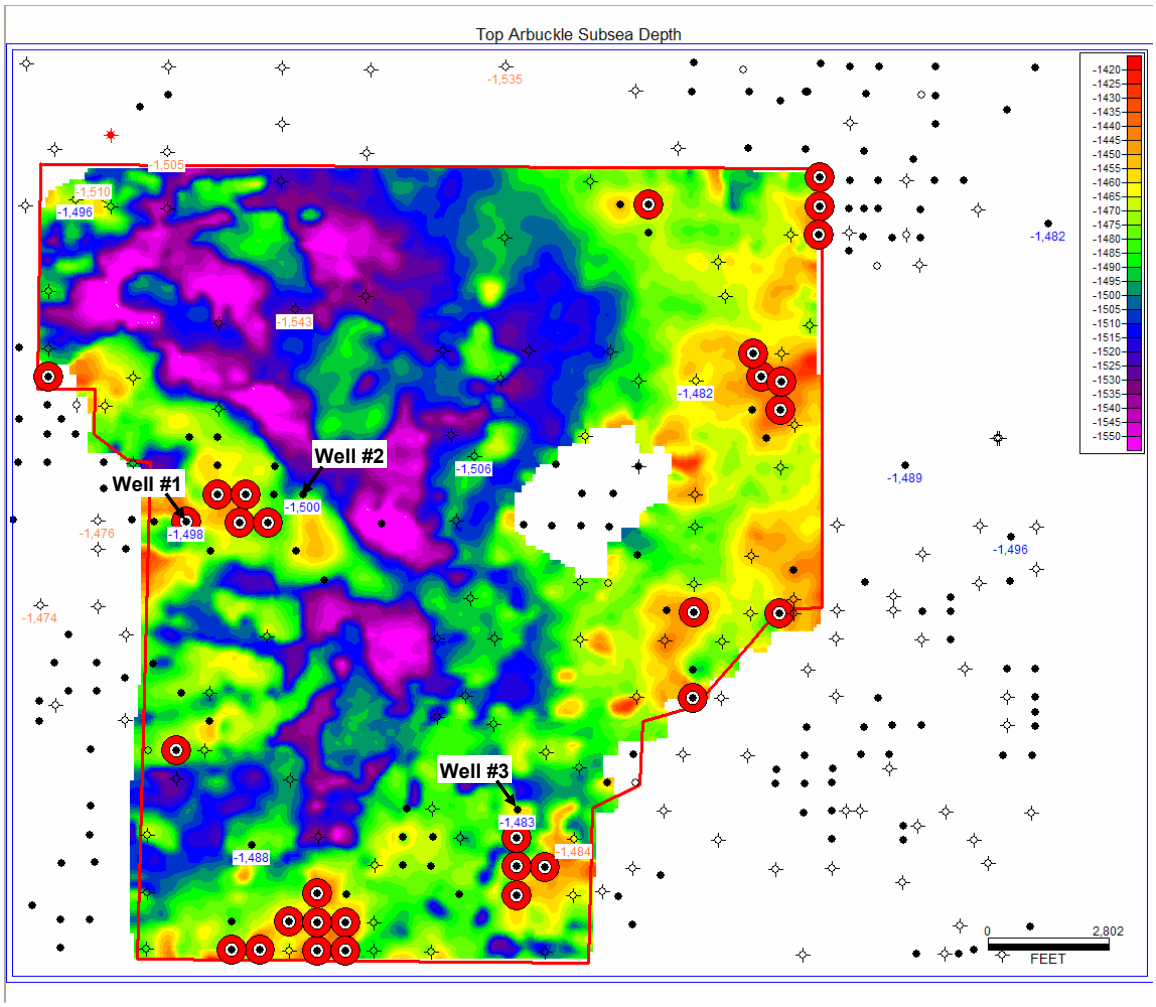

Figure 4.1. Top of Arbuckle depth map (in feet subsea), constructed using 3-D seismic interpretations and well tops. The subsea depths (in feet) of the oil/water contact from wireline log interpretations (blue) and ACO-1 reports (orange) are posted at well locations. Wells #1, #2, and #3 are discussed in the text. Wells that have produced from the Arbuckle are highlighted in red.

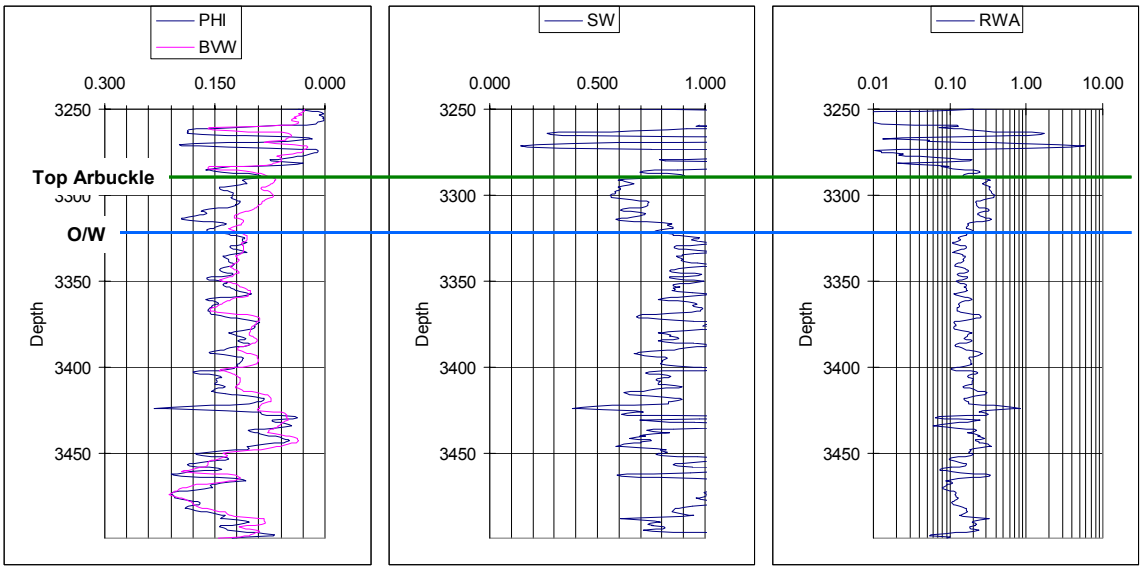

Figure 4.2. Porosity (PHI), bulk volume water (BVW), water saturation (SW), and apparent resistivity (RWA) for well #1, showing the position of the oil/water contact.

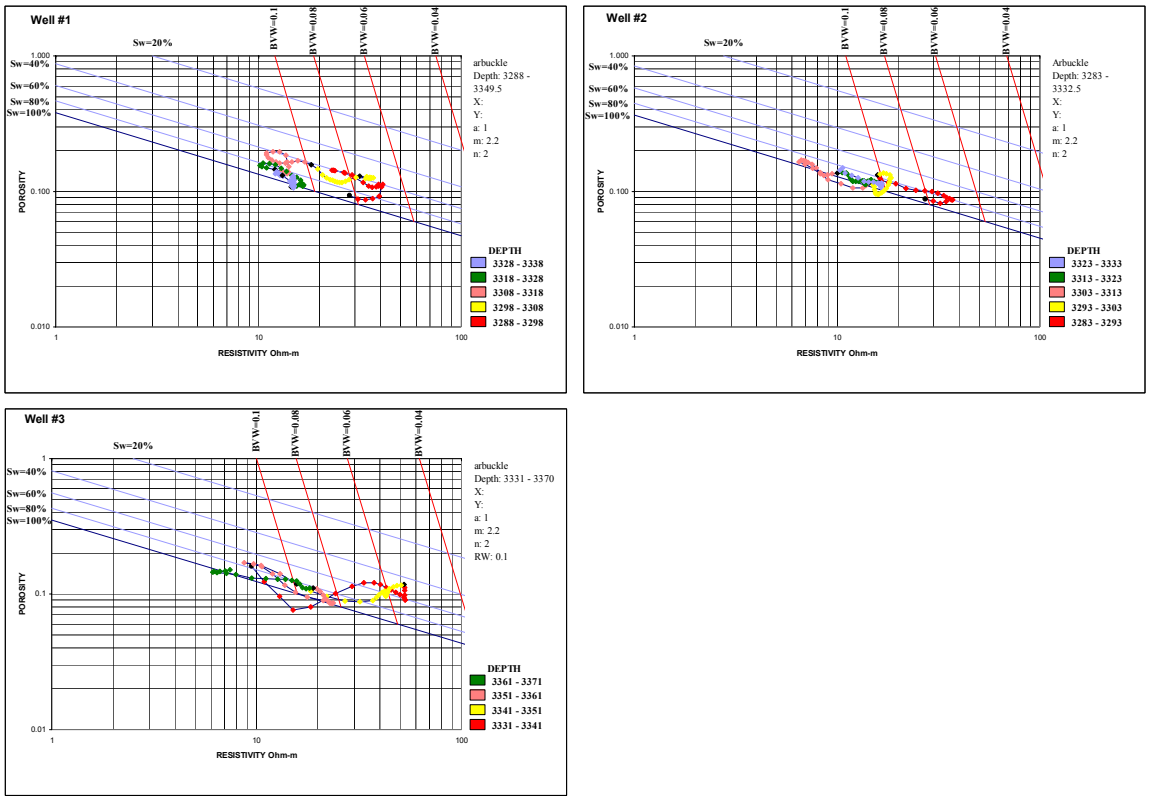

Figure 4.3. Pickett plots for three wells within the Arbuckle study area. Points are plotted at 0.5 ft intervals. Well locations are shown in Figure 4.1.

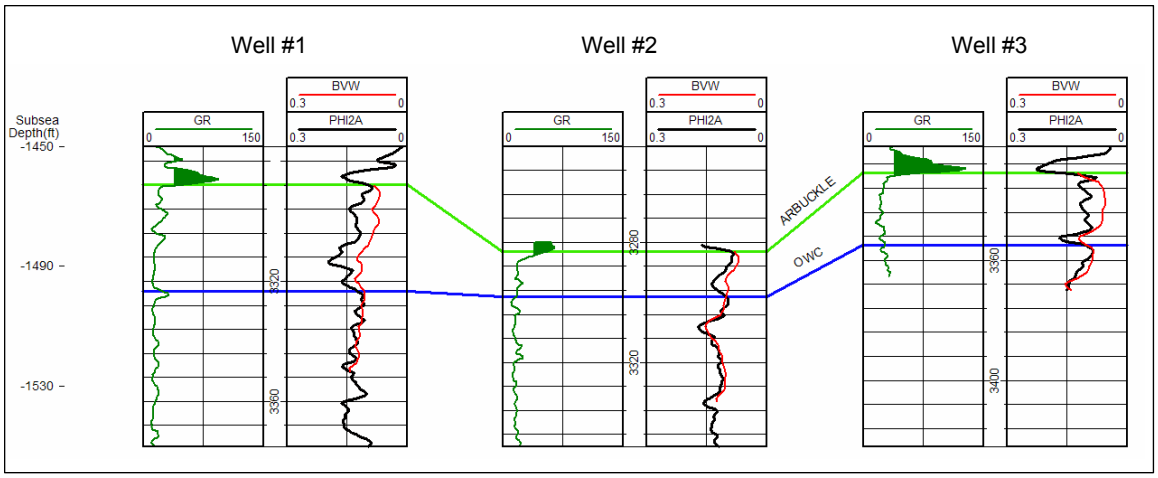

Figure 4.4. Gamma ray (GR), average neutron-density porosity (PHI2A), and BVW log cross section for the three wells shown in Figures 4.1 and 4.3.

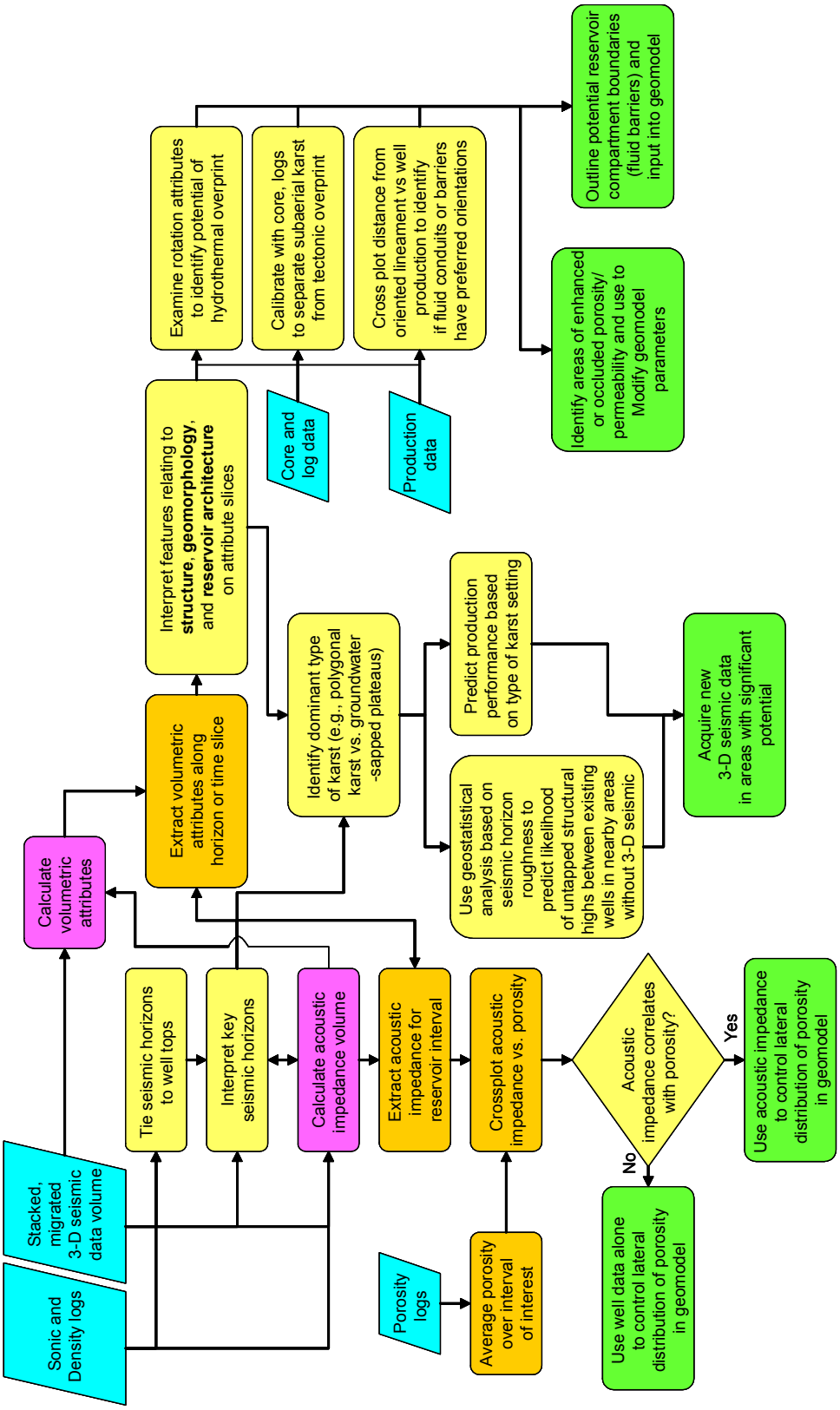

Figure 5.1. Generalized volumetric seismic attribute workflow for recognizing and interpreting data from karst-overprinted reservoirs. Colors indicate input data (cyan), generation of new data volumes (magenta), data extraction (orange), interpretation (yellow), and suggested use of results (green).